



Diopside + F-rich phlogopite at high P and T: Systematics, crystal chemistry and the stability of KMgF_3 , clinohumite and chondrodite

George E. Harlow

Department of Earth and Planetary Sciences,
American Museum of Natural History, New York, NY 10024-5192
USA <gharlow@amnh.org>

Abstract

Multianvil experiments have been carried out from 3.0 to 11 GPa and from 1100 to 1500°C on an equimolar mixture of natural diopside ($\text{CaMgSi}_2\text{O}_6$) and F-rich phlogopite ($\text{K}_{1.7}\text{Na}_{0.24}\text{Mg}_{5.6}\text{Al}_{2.4}\text{Si}_{5.8}\text{O}_{20}[\text{F}_{1.7}\text{OH}_{2.3}]$) to examine the behavior of K and F at high P and T in this system. As the first extensive experiments in the KCMASH composition space to include fluorine, the subsolidus crystallization of the perovskite KMgF_3 and F-bearing clinohumite and chondrodite at high pressures, up to 10 GPa and 1400°C, is noteworthy. The compositions of crystalline phases produced in the experiments vary systematically with P and T. In clinopyroxene: Kcpx (KAlSi_2O_6) content in clinopyroxene increases with increasing pressure at pressures above 5 GPa without a noticeable temperature effect; CaTs ($\text{CaAl}_2\text{SiO}_6$) content is negatively correlated with P above 3 GPa and is positively correlated with T. In amphibole – an $^{\text{M4}}\text{K}$ -substituted potassic richterite, ideally $\text{K}(\text{KCa})\text{Mg}_5\text{Si}_8\text{O}_{22}(\text{OH},\text{F})_2$: K content is positively correlated with P; Al and F content decrease with P; and F content is positively correlated with T and is lowered by coexisting KMgF_3 . In garnet: ^{6}Si and Na content increases upon increasing P; Ca-Mg systematics are complicated by growth zoning of crystals. All of the above trends may merit further calibration in geobarometry above 6 GPa, where published Al-in-Opx and Opx-Cpx barometers fail for these experiments. Although fluorine content in hydrous minerals decreases upon increasing P, fluorine enlarges the high P-T stability field of the hydroxy-minerals, so F content, even at low levels, must be considered in modeling phase stabilities for mantle assemblages. However, the strictly subsolidus paragenesis of humites in these experiments adds to the evidence that mantle humites form via metasomatic rather than magmatic interactions.

Keywords: potassic richterite, potassic clinopyroxene, KMgF_3 , clinohumite, chondrodite, fluorine, experimental study, high pressure.

Introduction

Potassium and other large-ion lithophile elements undoubtedly played an important role in the differentiation of Earth and continue to be important in the processes of subduction, mantle plume formation, mantle metasomatism, upper-mantle melting, and Earth's heat budget, due to ^{40}K . Consequently, considerable effort has been exerted in recent years to understand the behavior of large-ion lithophile elements, like potassium, in Earth's interior. Studies range

from experimental examinations of potential stable host minerals, e.g. K in clinopyroxene (Edgar and Vukadinovic, 1993; Harlow, 1997; Luth, 1997) or potassic phases (e.g. Trønnes, 1990; Sudo and Tatsumi, 1990; Foley, 1991; Yagi et al., 1994; Luth 1997; Konzett et al., 1997; Inoue et al., 1998; Konzett and Ulmer, 1999; Konzett and Fei, 2000), to the fate of enriched subducted slab components (e.g. Massone, 1992; Irifune et al., 1994; Schmidt, 1996; Konzett and Fei, 2000); or melting of fertile or enriched peridotites (e.g. Mitchell, 1995; Tsuruta and Takahashi, 1998; Wang

and Takahashi, 1999). These experiments have demonstrated the significant stability of ^{M4}K -substituted potassic richterite ($(K(KCa)Mg_5Si_8O_{22}(OH)_2$ – sometimes referred to as KK-richterite), the enrichment of K in clinopyroxene (cpx) above 5 GPa, and the existence of the high-pressure phases K-hollandite [$KAlSi_3O_8$] and phase-X [$\square_x K_{2-x} Mg_2 Si_2 O_7 H_x$].

I started multianvil experiments with mixtures of diopside + phlogopite to reproduce ^{M4}K -substituted potassic richterite as described by Sudo and Tatsumi (1990) for structure refinements because K substitution into the M4 site of amphibole is analogous to its substitution into the M2 site of cpx as inferred and then described in our studies (Harlow and Veblen, 1991; Harlow, 1996). With the paucity of studies involving fluorine in lieu of hydroxyl, I used a F-rich phlogopite in the experiments to make them more revealing, given the focus of other workers on F-free systems. Although the structure of ^{M4}K -substituted potassic richterite has now been refined by Yang et al. (1999), the experiments have yielded a wealth of information on crystal chemistry and phase assemblages and on the stabilization of F-bearing humite-group minerals and the perovskite phase $KMgF_3$.

Experimental and Analytical Methods

The starting materials for the experiments were equimolar mixtures of natural F-rich phlogopite (Phl), $K_{1.7}Na_{0.24}Mg_{5.6}Al_{2.4}Si_{5.8}O_{20}(F_{1.7}OH_{2.3})$ (AMNH 35777, Edenville, NY) and diopside, $CaMgSi_2O_6$, (AMNH 39849, Diopside, Wakefield Quarry, Quebec) (see Table 1). Defining one mole of phlogopite with 20 oxygens (exclusive of OH and F) as opposed to 10 doubles the amount of alkalis and univalent anions in these experiments relative to those of Sudo and Tatsumi (1990) and Luth (1997). Natural minerals provide adequate amounts of both F and H_2O to the experiments plus important minor elements such as Na, Ba, and Fe which manifest important crystallochemical preferences in the experiments. Phlogopite was powdered by filing a large book using a diamond file and diopside was ground in an agate mortar, yielding fragments smaller than 100 μm . The powders were weighed and mixed by lightly regrinding for several minutes in a mortar. Aliquots of powder were packed (approx. 10 mg) into platinum capsules that were crimped and welded shut. The capsule with an alumina jacket was placed in contact with a D-type (W3%Re/W25%Re) transversely-mounted thermocouple (Tc) inside of a $LaCrO_3$ cylindrical heater in an octahedron with integral fins molded from castable ceramic. Experiments were performed in a Walker-style multianvil press following the procedure described by Harlow (1997). Conditions for experiments cited here are given in Table 2, and range

Table 1. Analyses of starting materials and bulk compositions from this and related studies¹.

Exper.	Di	Phlog	Bulk	Bulk A	Bulk B	Bulk C
SiO ₂	55.50	42.11	44.83	49.35	47.28	45.35
TiO ₂	0.03	0.13	0.11	-	-	0.12
Al ₂ O ₃	0.04	14.35	11.27	6.10	11.50	4.37
Cr ₂ O ₃	0.00	n.d.	0.00	-	-	0.69
Fe ₂ O ₃ *	0.08	0.00	0.02	-	-	-
FeO	0.04	0.81	0.65	-	-	6.95
MnO	0.02	0.02	0.02	-	-	0.08
MgO	18.60	27.13	25.23	23.80	27.26	37.24
CaO	26.00	0.01	5.53	12.96	6.58	3.55
BaO	0.00	0.47	0.37	-	-	-
Na ₂ O	0.03	0.88	0.70	-	1.22	0.69
K ₂ O	0.00	9.64	7.57	5.64	4.94	0.54
F	0.00	3.86	3.03	-	-	-
H ₂ O	-	2.48†	1.95	2.15	1.22	0.21
O=F	-	-1.63	-1.28	-	-	-
Total	100.34	100.24	100.00	100.00	100.00	100.00
Oxygens	6	20	6	(exclusive of OH)		
Si	1.996	5.859	1.620			
^[4] Al	0.002	2.141	0.480			
Ti	0.001	0.014	0.003			
^[6] Al	0.000	0.213	0.000			
Cr	0.000	-	0.000			
Fe ³⁺ *	0.002	0.000	0.000			
Fe	0.001	0.094	0.020			
Mn	0.001	-	-			
Mg	0.997	5.629	1.360			
Ca	1.002	0.001	0.214			
Ba	0.000	0.025	0.005			
Na	0.002	0.236	0.049			
K	0.000	1.712	0.349			
H			0.470			
Total	4.003	15.924	4.225			
F	-	1.700	0.346			
OH†	-	2.300	-			

¹ Bulk A for Sudo and Tatsumi (1990) and Luth (1997); Bulk B for subalkaline KNCMASH composition of Konzett and Ulmer (1999) and Konzett and Fei (2000); Bulk C for Modified Brian 2 plus Phl of Konzett and Ulmer (1999).

* Fe³⁺ determined by cation sum and charge balancing.

† H₂O and OH estimated by calculating 4 univalent anions (F+OH) in mica.

from pressures just below the first reaction of Di + Phl, ~ 3 GPa, to the limits of the castable ceramic technique, ~12 GPa, and from 1100 to 1500°C. Some early experiments were initially overheated (e.g. BB438, GG524, TT270, GG748) for 1 hour and then lowered manually

Table 2. List of experiments, conditions, and resulting assemblages.

Exper.	Hrs	Load	P GPa	T °C	T last	Coexisting Phases ¹
TT346	28	172T8	3.8	1100	1100	Cpx, Phl
TT321	25	210T8	4.6	1100	1100	Cpx, Phl, Grt?, Q
TT352	24	363T8	8.0	1100	1100	Cpx, Phl, Amph, Grt, Chn, KMgF ₃
TT350	27	255T6	8.7	1100	1100	Cpx, Amph, Grt, Chn, KMgF ₃
TT353	24	325T6	10.8	1100	1100	Cpx, Amph, Grt, Chu
TT320	24	172T8	3.8	1200	1200	Cpx, Phl, Gl
BB438	24	366T8	8.1	1400	1200	Cpx, Grt, Amph, Chn, KMgF ₃ ; Cpx, Grt, Q
GG738†	24	227T8	5.0	1400	1200	Q/HiCaCpx, Phl, Grt, Fl, LoCaCpx, En
BB173	24	309T8	6.8	1200	1200	Cpx, Phl, Grt, Chn, KMgF ₃
TT298*	24	289T6	9.7	1200	1200	Cpx, En, Phl, Grt, Q
GG765	24	298T6	9.9	1200	1200	Cpx, Grt, Amph, Chu, KMgF ₃
GG746	24	233T8	5.1	1400	1300	Cpx, Phl, Grt, Q
BB361	19	307T8	6.8	1400	1300	Cpx, Grt, Phl, Chu, KMgF ₃ ; Cpx, Grt, Phl, Q
GG524	19	405T8	8.9	1400	1300	Cpx, Grt, Amph, Fo; Cpx, Grt, Q (KMgF ₃)
BB692	24	295T6	9.8	1300	1300	Cpx, En, Fo, Grt, Amph, KMgF ₃
GG748	6	236T8	5.2	1500	1400	Cpx, Grt, Fo, Phl?; Cpx, Grt, Q (Phl, En, KMgF ₃)
TT286	24	275T8	6.1	1500	1400	Cpx, Phl, Grt, Fo; Cpx, Phl, Grt, Q
BB170	24	291T8	6.4	1469	1400	Cpx, Grt, Fo, Q
TT270	24	305T8	6.7	1500	1400	Cpx, Grt, Amph, KMgF ₃ , Fo; Cpx, Grt, Q
BB709	24	241T6	8.5	1400	1400	Grt, Gl, Q
BB705	24	305T6	10.5	1400	1400	Cpx, Grt, En, Amph?, KMgF ₃ ; Cpx, Grt, Q (Amph, KMgF ₃)
BB702	24	313T6	10.7	1500	1500	Cpx, Grt, Amph; Cpx, Grt, Q (Amph, KMgF ₃ , KBaCa-phase)
GG733	24	338T8	7.4	1600	1500	Cpx, Grt, Amph, Fo; Cpx, Grt, Q

¹ Phase abbreviations: Cpx—clinopyroxene, Grt—garnet, Amph—amphibole, Fl—fluorite, Fo—forsterite, Chn—chondrodite, Chu—clinohumite, Gl—glass, Phl—phlogopite, Q—quench (with identified phases in quench in parentheses)

* Something unknown went wrong with this experiment so that the pressure attained was not as high as inferred; it is retained to demonstrate that compositions of several phases indicate the lower pressure.

† This two stage experiment shows both early total melting and then crystallization, so it is in part presented as two experiments, one at 1400 and the other at 1200°C.

(in a few seconds) to the final T in an attempt to approach equilibria from higher temperature and create more reactive conditions. However, in these experiments there was some ambiguity about the final assemblages and garnets may have crystallized early and never re-equilibrated at the lower temperature (see below); so this processing was stopped midway through the project. No attempt was made to carry out reversed experiments; these are synthesis experiments always containing the initial phases diopside and phlogopite. Textures manifest the thermal structure of the assemblies with isotherms following a profile like an hourglass through the cap-

sules, such that quench melt, when it exists, forms convex intrusion into the Pt capsule from its walls (Fig. 1). As in Harlow (1997), temperature variation in the capsule is estimated as $\pm 25^\circ\text{C}$. Thermal compaction is a typical textural feature, most obvious as clustering of the liquidus phase (garnet at higher pressure) at the melt boundary where present.

Processed octahedral assemblies were imbedded in epoxy and sawn in half with a 4 mil diamond blade with mineral spirits as a lubricant (to prevent dissolution of any water-soluble phases). No attempt was made to quan-

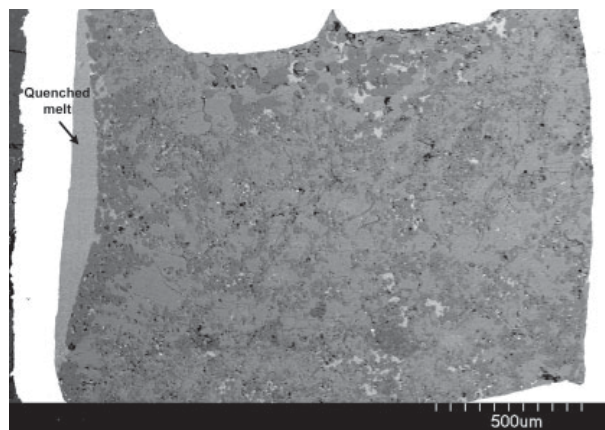


Figure 1. Back-scattered electron (BSE) micrograph of experiment TT270 demonstrating thermal structure within capsules and the thermal compaction at quenched-melt boundary to left. Phases in order of decreasing brightness are Pt capsule, KMgF_3 , quenched melt, Cpx, Amph, Grt, Fo, holes.

tify or sample fluid/water evolution in these experiments as little was expected and compositional variation among solid phases is my primary focus. One half of each experiment was polished on diamond-impregnated laps with mineral spirits for study of textures and compositions and the other half retained for potential extraction of contents. Polished samples were imaged using a Hitachi S-4700 FE scanning electron microscope with back-scattered electron BSE imaging and PGT-Imix energy dispersive x-ray spectrometer (EDS). Microprobe analysis of polished experimental products was carried out for constituent major elements except O using a Cameca SX100 operating at 15 kV and 10 nA sample current, employing a point beam for crystalline phases and a 10 μm diameter beam for glasses and quench products (those liquids that form very fine scale solid intergrowths upon quenching). Natural minerals were used as standards, and the PAP correction scheme according to Pouchou and Pichoir (1991) was employed. Potential interferences between Ba ($L\alpha$) and Ti ($K\alpha$) were minimized by measuring x-ray counts on a PET crystal and background outside the window of both peaks — as long as concentrations are as low as found in these experiments, there are no overlaps that exceed the detection limit. No interference was detectable on F ($K\alpha$) x-ray counts from a deposition pseudo crystal ($2D=45\text{\AA}$) by Fe ($L\alpha$); background likewise measured outside of Fe peak. For all elements except F and O, detection limits are <0.01 wt%; for F and O it is about 0.02 wt%; but “as measured” values are presented throughout the tables. No post processing correction was made for the effect of inferred water content. Crystalline phases are abbreviated in a capitalized form according to Kretz (1983) unless otherwise specified.

The tables of analyses require some explanation, particularly with respect to estimates of Fe^{2+} and Fe^{3+} , even though iron is a very minor element in these experiments. I use an algorithm similar in concept to Finger (1972) to calculate Fe^{3+} in which cation charge must sum as close as possible to twice the number of oxygens plus the number of univalent anions (e.g. 12 for 6 oxygens in pyroxene), with a maximum permissible sum of cations determined by the phase’s crystal structure (e.g. 4 for pyroxene as above; vacancies in large cation sites are permissible). So, Fe^{3+} is converted from available measured Fe (assumed Fe^{2+}) to attempt to account for deficient charge (or excess cations), extra O is added proportional to the Fe^{2+} converted to Fe^{3+} , and iteration of the new Fe^{3+} and O values into the calculation until convergence is achieved. Cations are then distributed in the several phases as Si and $^{[4]}\text{Al}$ into tetrahedral sites (T); excess Si, Ti, $^{[6]}\text{Al}$, Fe^{3+} , Fe^{2+} , Mg and sometimes Ca into 6-8 fold sites; and Na, K, Ba, and other times Ca into 8-12 fold sites, with cation sums noted as Sum T, for tetrahedral cations, and Total for total cations (except in the case of amphibole where A, B, and C sites are totaled separately).

Results

Phase Relationships

The results of the experiments are listed in Table 2 and plotted in Figure 2. The main caveats to phase assemblage identification are the difficulties in observing very small amounts of a phase and the potential complications of thermal gradients upon the determination of coexisting phases. As pointed out by Stalder and Ulmer (2001) in multianvil experiments on a serpentine composition, fluid migration and thermal-driven diffusion (and perhaps other factors) create chemical migrations so that the phase rule for a single bulk composition is violated; they resolve the problem via local assemblages with slightly different bulk compositions. Comparable variations occur in this study, but as the multicomponent system explored here is complicated, I have only attempted to describe the local assemblages. They are listed as the coexisting solid assemblages and/or the melt-solid assemblages in each Pt capsule (Table 2). For capsules with melt – supersolidus conditions – not all phases are in contact with melt; those “contacts” are described below. Upon increasing pressure, garnet first appears at just above 4 GPa followed by KMgF_3 at about 5 GPa and chondrodite at about 7 GPa, although they may appear over a smaller pressure range (or even simultaneously) and were just not identifiable. KMgF_3 occurs as an interstitial phase with other solids without any indication of being a quench product (Figure 3). KMgF_3 is stable through subsolidus conditions to at least 1400°C and 11

GPa. Amphibole appears at ~ 8 GPa and persists to the highest pressures below the solidus. Phlogopite reacts out at about 8 GPa, coexisting with amphibole over a narrow pressure range. The coexistence may extend over a larger pressure range at lower T and “wedge out” at higher T. These “in”/“out” reactions appear to have a slight negative P/T slope. Chondrodite is replaced by clinohumite at higher pressure followed by olivine with reaction boundaries that appear to have a steep negative P/T slope (~ 20 MPa/deg). Melting initiates at about 1150°C and 4 GPa with a steep positive P/T slope of (~ 35 MPa/deg). Because of thermal compaction, melt separates from solids so that determination of solidus phases can be difficult. Generally, garnets are concentrated at the melt solid boundary, so garnet is clearly a solidus phase, and it persists to the highest temperatures. At pressures below the Phl-out reaction, Cpx, Phl, and Grt are all in contact with melt. At pressures above that reaction, Cpx is also a solidus phase near the melting curve. In several experiments Kamph coexists with melt in the capsule, but it is never in contact with melt. In experiments BB705, BB702, and GG733 Kamph is within about a hundred micrometers of the melt boundary, so it may be just “off” the solidus at these conditions of higher P and T. Olivine is generally minor in abundance and tends to be in the colder portions of the capsules, so it appears to be a subsolidus phase. Although attempts were made to preserve subsolidus soluble phases such as KOH, it was not detected.

The experiments carried out in this study are most similar to those of Sudo and Tatsumi (1990) and Luth (1997) on F-free, synthetic (pure) Di + Phl, thus in the system $\text{K}_2\text{O}-\text{CaO}-\text{MgO}-\text{Al}_2\text{O}_3-\text{SiO}_2-\text{H}_2\text{O}$ (KCMASH), and have compositional similarities with those of Konzett et al. (1997) and Konzett and Ulmer (1999) employing both synthetic subalkaline “phlogopite peridotite” (with Na_2O and thus in KNCMASH) and a modified K-spiked spinel lherzolite (see Table 1). The results here are somewhat different from the previous studies. Garnet appearance is at least 1 GPa lower than in the studies cited above, except the KNCMASH results of Konzett and Ulmer (1999). KMgF_3 is a phase only reported once in high-pressure studies (Thibault, 1993) probably for lack of experiments on appropriate F-bearing compositions having reached suitably high pressure or resolution of such an unusual minor phase (e.g. Foley, 1990). The position of the subsolidus “Phl-out” reaction is comparable to that of Luth (1997), is at slightly higher P than in the phlogopite-doped lherzolite experiments of Konzett and Ulmer (1999), but is below the ~ 8.5 GPa for the KNCMASH experiments of those researchers. Sudo and Tatsumi (1990), on the other hand, placed the “Phl-out” reaction above 10 GPa. The narrow pressure range of coexisting Phl + K-rich amphibole (Kamph) is similar to the triangular stability field proposed by Luth (1997). Kamph appearance is at higher P than in other experiments except Luth (1997), and its stability to 1400°C supersolidus is also higher. A significant difference for the experiments

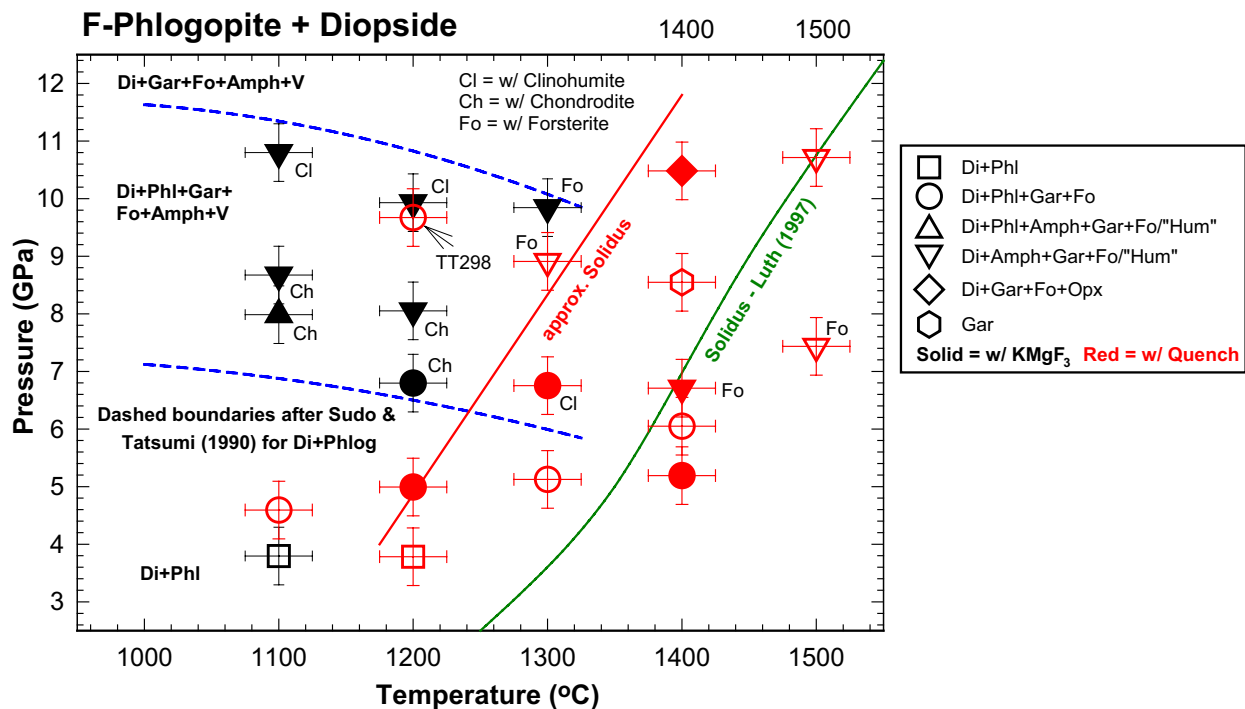


Figure 2. Pressure-temperature diagram of experimental results.

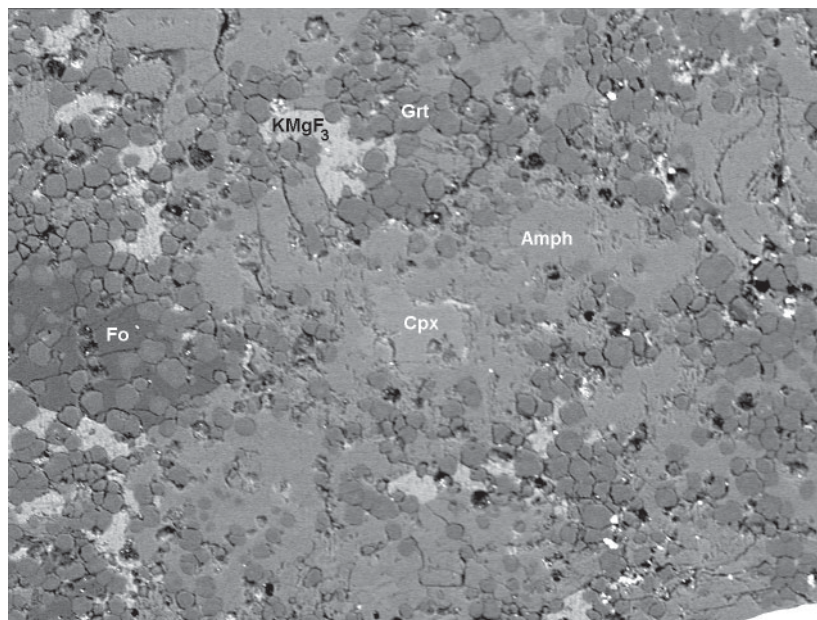


Figure 3. BSE micrograph (500 μm wide) of central portion of experiment TT270 showing coexisting KMgF_3 , cpx, amphibole, garnet, and forsterite. Bright spots are brass contamination entrained during polishing of sample in brass mount.

reported here is the appearance of humite minerals at the expense of forsterite below 1200°C, which should be due to the presence of fluorine. Finally, the solidus follows a similar positive slope to that in other experiments (e.g. Konzett and Ulmer, 1999) but may be 100°C lower than that in Luth (1997).

Mineral compositions

KMgF_3 . This perovskite phase, the K-analog of neighborite – NaMgF_3 , has been used extensively as a model for silicate perovskite (e.g. Zhao et al., 1990) but is not known in nature and has only been reported in geologically-focused experiments by Thibault (1993). For most experiments, analyses of KMgF_3 include some overlap with adjacent silicates, so only a few better analyses of larger grains are reported in Table A1. Compositionally, in addition to its essentially stoichiometric character, KMgF_3 is also a limited sink for Na and Ba. The minor amount of O (oxygen was measured for this phase) is not balanced by measured cations but varies reciprocally with F, so OH may be a reasonable interpretation. FT-IR verification has not been undertaken.

Phlogopite. The natural phlogopite used as starting material in this study contains Na, some octahedral aluminum ($^{[6]}\text{Al}$), and tetrahedral aluminum ($^{[4]}\text{Al}$) in excess of 2.0 atoms per formula unit (apfu – see Table 1), so some attention was paid to recognizing compositional changes from possible relict phlogopite with its distinctive levels of minor elements. Compositions of mica from the experiments are listed in Table A2. The mica pro-

gressively reacts and recrystallizes even at the lowest P and T explored. One example is that the minor Na content decreases below its starting composition value upon increasing P to 5 GPa and remains approximately constant at 0.2 apfu (Fig. 4a) at higher P. The K content, on the other hand, initially increases upon increasing P to 5 GPa and, then, remains essentially constant at 1.92 apfu at higher P. These changes show that the phlogopite is not relict, and the compositions are consistent with the results of Konzett and coworkers. Ba content of phlogopite remains essentially constant, although there may be a slight indication of decrease upon increasing P. The trend for $^{[4]}\text{Al}$, which just happens to match the starting composition value at ~4 GPa and 1100°C, smoothly decreases to 1.76 apfu upon increasing P prior to the “Phl-out” reaction (Figure 4b). A similar decrease in $^{[4]}\text{Al}$ was reported in other experimental studies and is ascribed to the effect of pressure, Al uptake by garnet formation, and Al+Na incorporation as jadeite content in cpx. The content of $^{[6]}\text{Al}$ is very minor and shows considerable variation at 5 GPa but decreases at higher P (Fig. 4c). Fluorine generally increases upon increasing P (and probably T) to about 6 GPa and then drops to roughly its “starting” value (Fig. 4d), which can only be a coincidence as the Phl is not unreacted. Competition for F may be the cause, by KMgF_3 as it increases in abundance as well as by crystallization of Kamph. In either case, the decrease in F in Phl belies the interpretation that pressure stabilizes F-phlogopite over OH-phlogopite. So, the major changes upon increasing pressure appear to be driven by Al and Na reacting into garnet and pyroxene, and phlogopite

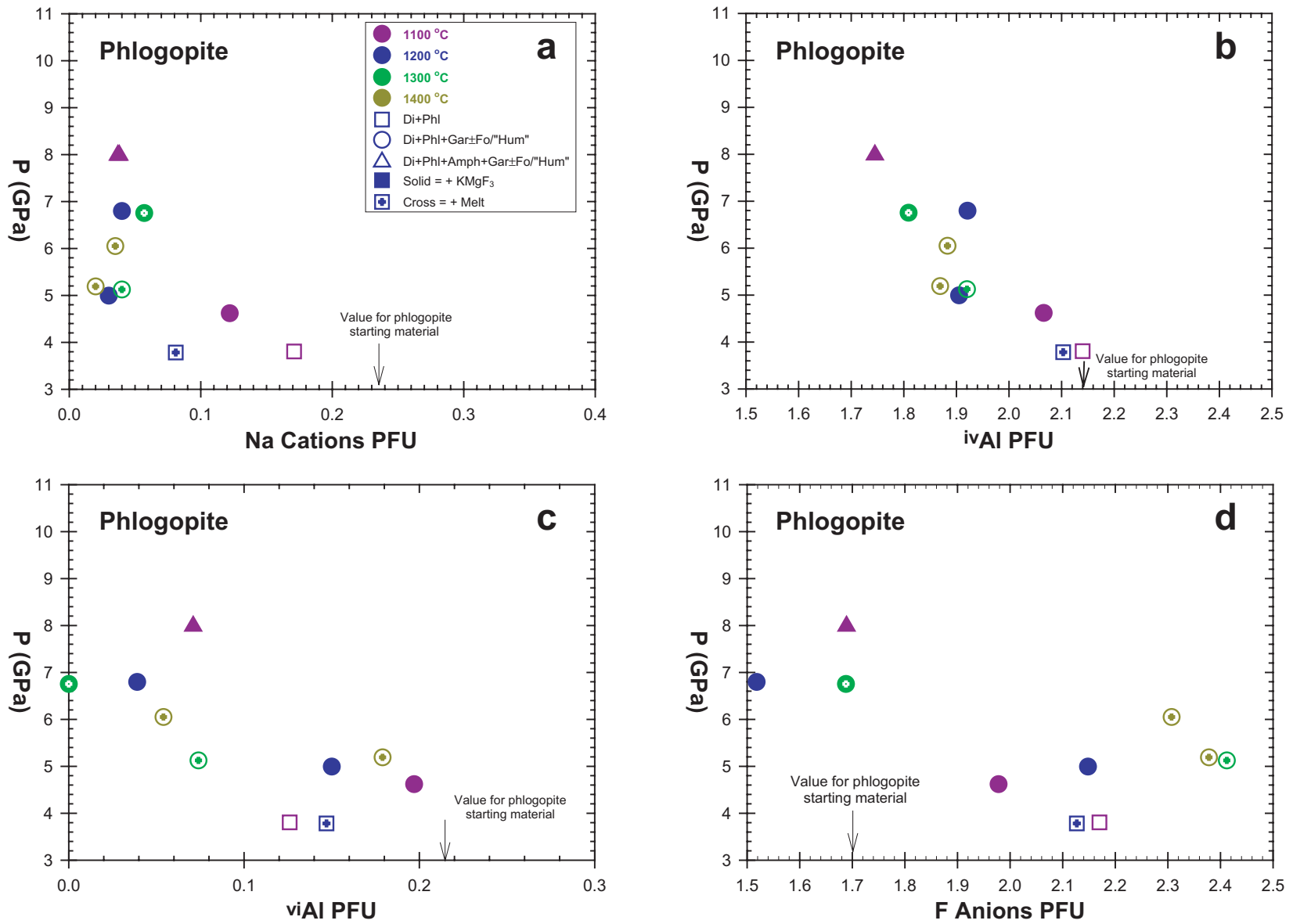


Figure 4. Scatter plots of aspects of phlogopite composition from experiments. a) Na versus P; b) ^{iv}Al versus P; c) ^{vi}Al versus P; and d) F versus P.

breakdown coupled to formation of KMgF_3 with its preference for F over mica.

Amphibole. The amphibole that forms is the variety of K-rich richterite in which about 50% of the M4-site is filled by K, first observed by Sudo and Tatsumi (1990) and Trønnes (1990), ideally $\text{K}(\text{KCa})\text{Mg}_5\text{Si}_8\text{O}_{22}(\text{OH},\text{F})_2$. It is important as a carrier for water and potassium at mantle conditions with the incorporation of K into M4 of the amphibole structure being crystallochemically similar to K entering the M2 site of clinopyroxene at high pressure (e.g. Harlow, 1996). Compositions of K-rich amphiboles from the experiments are presented in Table A3. K-rich amphibole forms at about 8 GPa and 1200°C with 1.4 K apfu, which increases upon increasing P to 1.8 apfu at the limit of the experiments at ~11 GPa and 1500°C (Fig. 5a). The increase of K content upon increasing P at constant T is consistent with the results of Konzett and Ulmer (1999). There are some, but inconsistent, data to suggest K content decreases upon increasing T at constant P, K varying by 0.2 apfu over 400° (see Fig. 5a). Na content is small, 0.3-0.4 apfu, and is essentially constant throughout the experiments, suggesting equal compatibility with Cpx and melt/fluid in the amphibole stability field. The cation sum essentially equals 16 apfu for amphiboles, requiring an absence of vacancies and an A site fully occupied with potassium. Total Al content generally decreases upon increasing P, as noted by Konzett and Ulmer (1999) and Konzett et al. (1997), although the data are not fully consistent (Fig 5b). Fluorine content appears to decrease upon increasing P, increase upon increasing T, and is consistently lower in assemblages where KMgF_3 is present. This fluorine trend contrasts somewhat from the stability experiments of Foley (1991) which showed higher T stability for K-rich richterite and perhaps higher P stability; unfortunately compositions were not recorded in this study to assess possible changes in composition.

The Kamph compositions reported here fill the gap between the studies of Luth (1997) – only one composition reported, Konzett and Ulmer (1999), and Konzett et al. (1997) – with lower K-rich amphibole content, and Sudo and Tatsumi (1990) – with nearly ideal endmember K-rich amphibole. The generally higher K content reported here is due to higher bulk K_2O content (Table 1).

Garnet. Garnet compositions are listed in Table A4. Some aspects of garnet compositions are difficult to compare with those of other multianvil studies. Konzett and Ulmer (1999) noted that larger garnet crystals ($\geq 20 \mu\text{m}$) manifest higher Al and Ca contents in cores, but otherwise no crystal zoning is reported in previous studies. I find that garnets in some experiments, particularly lower

T/P or two T-stage ones (see above), are zoned such that cores are Ca-rich and rims are Mg-rich, and, particularly in two stage experiments, two growths are recorded in garnet. For example, in experiment GG524, larger garnets formed near the melt boundary – the hotter, more-reactive and volatile-enriched part of the experiment – have zoning from Ca-rich cores (~5 wt% CaO) to Mg-rich mid zones (~1.5 wt% CaO) which then have an overgrowth of Ca-rich garnet (~6 wt% CaO) and outer rims of Mg-rich garnet (~1.6 wt% CaO), recording two distinct episodes of zoned-garnet growth during the two stage experiment. Alternatively, in experiment BB705 at 1400°C, containing garnets over 100 μm in diameter, very little zoning is observed (e.g. the Mg cation content is 5.61 with s.d. of 0.023) from core to rim. Growth zoning and difficulty in obtaining analyses at garnet rims leads to apparent scatter in Ca (or Mg) in garnet among the experiments (Fig. 6a) and some contamination from melt for small garnets in TT353. However, there is only a small variation in Al content and the slightest variation in Si among the garnet compositions in a single experiment, e.g. GG524 (Fig 6b), but Mg and Si do vary inversely to Ca, Al, and Fe. Garnet is undoubtedly the most refractory of the experimentally-produced crystalline phases and fails to re-equilibrate except, perhaps, at rims. So, although multiple compositions are listed and plotted, only the rims of large garnets may represent the final conditions. Beyond these variations within experiments, it is difficult to define any trends of Ca or Mg with changing P and T.

Among the experiments there are systematic variations of some other elements in garnets. Si content increases above 6 apfu upon increasing pressure (Fig. 6c) which indicates formation of majorite and other $^{[6]}\text{Si}$ -containing components in the garnets, as has also been discussed by Luth (1997), Konzett and Ulmer (1999), and others discussed therein. Na follows a similar and better behaved trend with pressure (Fig. 6d) and indicates that about 20% of the $^{[6]}\text{Si}$ -containing garnet component is $\text{NaMg}_2^{[6]}\text{Al}^{[6]}\text{Si}_3\text{O}_{12}$. Errant points on this and other plots are from experiments at 1100°C where garnets are small and few analyses constrain the compositions adequately.

Clinopyroxene. Because diopside is used as a starting material, larger Cpx crystals in the capsules typically have a core of unreacted pure diopside. However, these cores are easily differentiated from overgrowths and new crystals, which have different compositions, and are interpreted as the equilibrium Cpx in the final assemblages. The exception is at low T and high P (e.g. experiment TT350) where compositional trends indicate that new crystals are too miniscule to be measured with the mi-

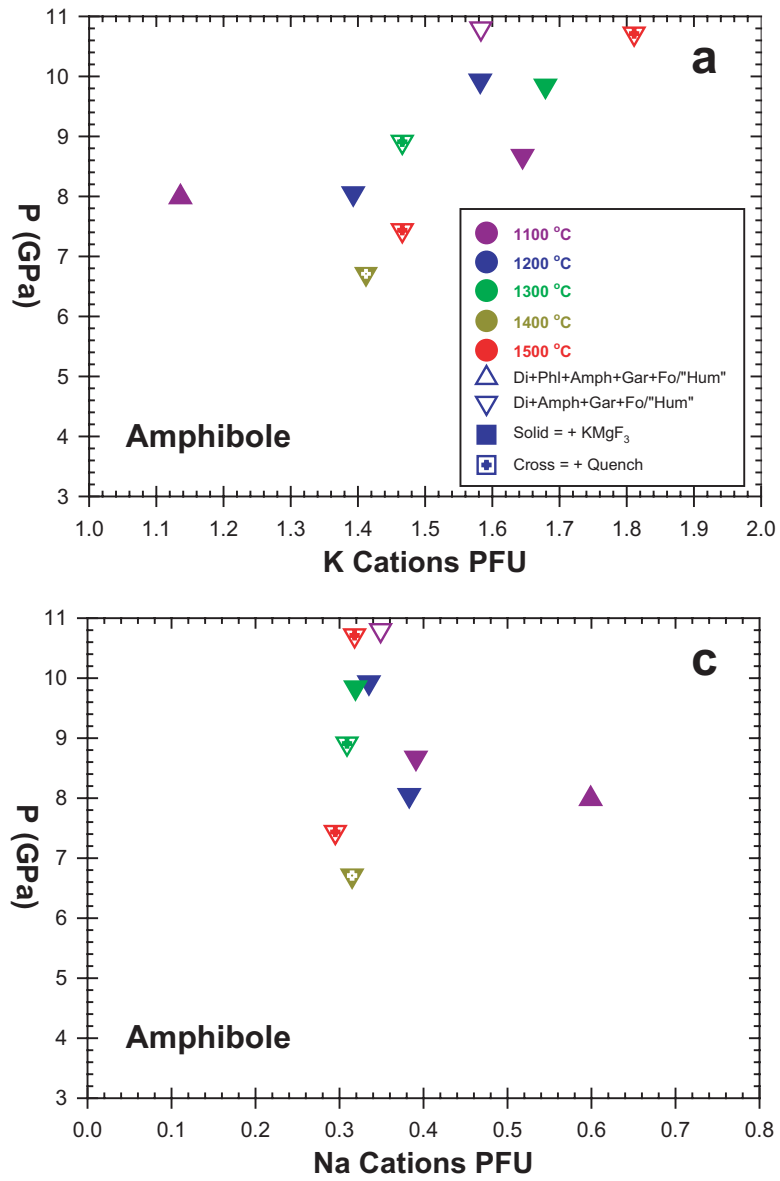


Figure 5. Scatter plots of aspects of amphibole composition from experiments. a) K versus P; b) Al versus P; c) Na versus P; and d) F versus P.

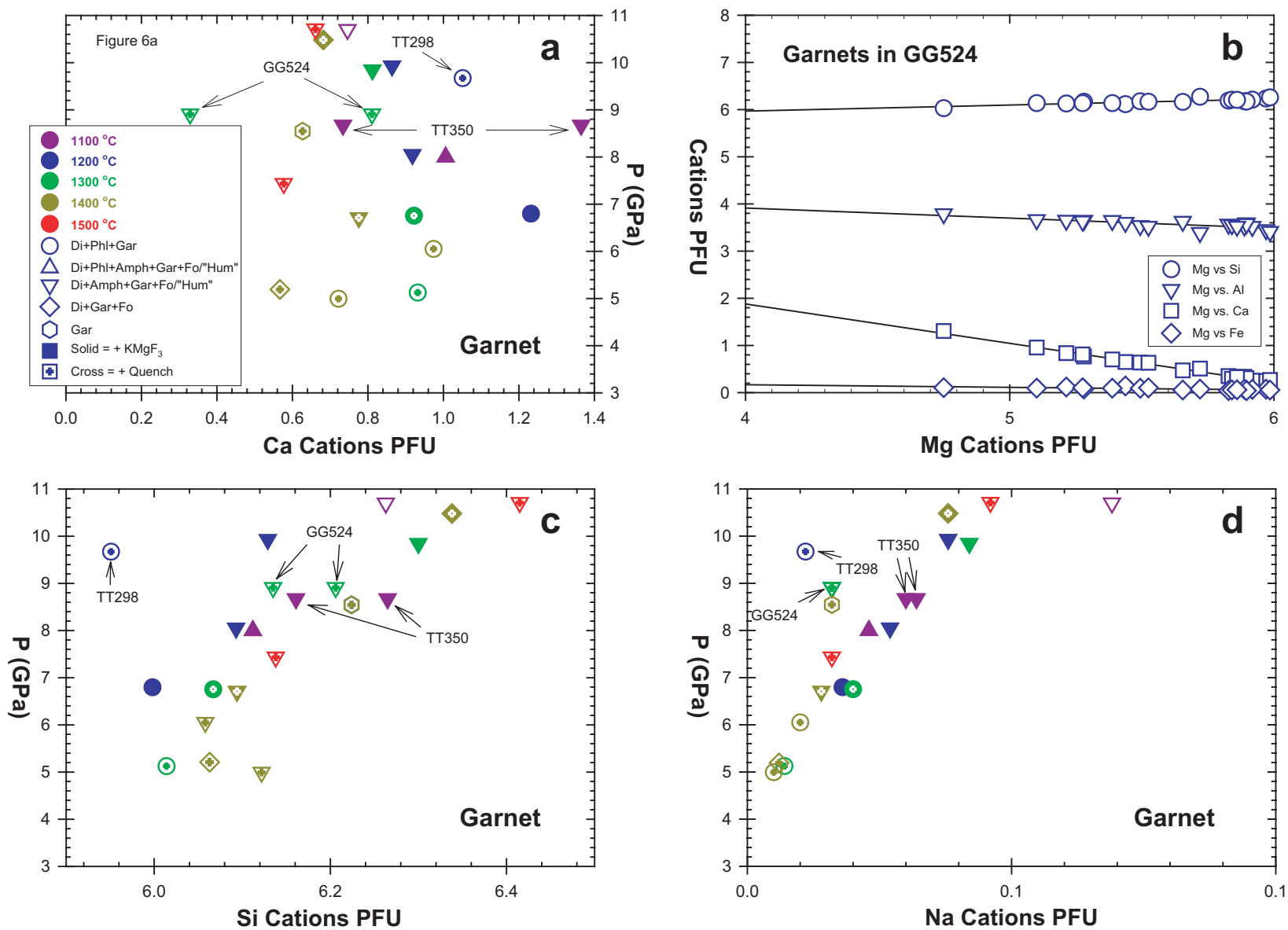


Figure 6. Scatter plots of aspects of garnet composition from experiments. a) Ca versus P; b) Mg versus Si, Al, and Ca in experiment GG524; c) Si versus P; d) Na versus P.

croprobe. Compositions are presented in Table A5. Cpx compositions compare well with the results of previous high-P experiments in systems with elevated K content. Kcpx (KAlSi_2O_6) content becomes measurable at about 4 GPa and increases upon increasing pressure without a consistent effect of temperature (Fig. 7a). There is not a clear relationship between Kcpx content and coexisting phases. Na content, on the other hand, is far more variable, perhaps increasing up to 5 GPa and then remaining relatively constant at higher P (Fig. 7b). As the Jd component is highly compatible at the pressures of these experiments, this variation indicates early Cpx scavenging of Na from Phl breakdown but, at higher P, relatively constant partitioning relative to Kamph. Calcium Tschermaks content ($\text{CaTs} - \text{Ca}^{[6]\text{Al}^{[4]}\text{AlSi}_2\text{O}_6}$) is highest (~0.9 mol%) at the lowest pressures with highest temperatures in these experiments and then drops off dramatically to negligible values above 8 GPa (Fig. 7c), which is consistent with previous work by Harlow (1999) and Luth (1997; not commented upon but data are shown in Fig. 7c). As the Cpx crystals in these experiments have effectively no vacancies (cation sum per 6 oxygens equals 4), there is no indication of any calcium Eskola pyroxene ($\text{CaEs} - \text{Ca}_{0.5}\square_{0.5}\text{AlSi}_2\text{O}_6$) content (see Harlow, 1999, and Gasparik, 1986). Enstatite plus ferrosilite components (Fe is treated as an addition to the $(\text{Mg,Fe})_2\text{Si}_2\text{O}_6$) are generally between 10 and 20% without any recognizable trend with respect to P; however at constant P, En+Fs appears to increase upon increasing T (Fig. 7d). Diopside content is fairly uniform at about 80 mol% suggesting a reciprocal balance in P- and T-sensitive solubilities with other components. For example, Kcpx content varies nearly inversely with CaTs as P changes, and, when account is taken of the T-sensitive solutions with CaTs and En, yields the stable Di content. Indeed, these reciprocal solubilities may also lead to the lack of recognizable T-sensitivity in the strongly P-dependent solubility of Kcpx in diopsidic Cpx.

Enstatite. The extraordinarily high Al contents in En from experiments GG738 and GG748 are interpreted as resulting from quench crystallization. Experiment GG738 was unusual in that it produced both a ripened quench texture on annealing at 1200°C as well as three pyroxenes: a high-calcium cpx, a low-calcium cpx, and enstatite (see Table A5). Enstatites found in other experiments have low Al content, are more consistent with equilibrium (see discussion), and can be used to evaluate the pressure for experiment TT298.

Olivine and humite-group minerals. Olivine is restricted to those experiments either at $1200 \leq T < 1400^\circ\text{C}$ containing amphibole + melt or at $T \geq 1400^\circ\text{C}$ containing melt. Otherwise “olivine” is represented by either

chondrodite, $(\text{Mg}_2\text{SiO}_4)_2 \cdot \text{Mg}(\text{F,OH})_2$, or clinohumite, $(\text{Mg}_2\text{SiO}_4)_4 \cdot \text{Mg}(\text{F,OH})_2$, stabilized here undoubtedly by the presence of fluorine as none of the similar experiments by others yield a humite mineral. Olivine is essentially stoichiometric (Table A6) except for very minor F content, which I interpret as minor substitutions by the humite exchange mechanism $^{[4]}\square(\text{OH,F})_4\text{Si}_{1-1}\text{O}_{-4}$ (see Ribbe, 1980) into the olivines grown in those experiments. Chondrodite and clinohumite were recognized by their substantial F content, low oxide totals and Mg/Si ratios, close to 2.5 and 2.25, respectively. Their analyses, although of limited quality and quantity in some cases, due to small size and/or few grains, match well with those of these minerals from low-Ti environments (e.g. metasomatized carbonates; Deer et al., 1982; Satish-Kumar and Niimi, 1998), both in the range of F contents and Mg/Si or the similar ratio for octahedral cation ($M_T = \text{Mg} + \text{Ti} + \text{Fe} + \text{Ca}$) and Si. Because only trace Ti is in the experiments, it is not possible to examine the systematics of $\text{TiO}_2 \rightleftharpoons \text{Mg}(\text{F,OH})_2$ exchange, which stabilizes natural humites at high P and T (e.g. Dymek, et al. 1988). Nonetheless, Ti is relatively high in the humites (~0.2 wt%), only matched in quench. With respect to crystallochemical trends, these few data have limited interpretability: F content (as apfu or the fraction of F/(F+OH)) in chondrodite and clinohumite decreases upon increasing P, with the exception of experiment TT353, and ambiguous variation with T (Fig 8a). There is an indication of increasing M_T/Si with increasing F (Figure 8b), which might be caused by increasing numbers of $\text{Mg}(\text{F,OH})_2$ units/“brucite”-layers in partially averaged structures of humite-group type, possibly transitional to Phase A ($\text{Mg}_7\text{Si}_2\text{O}_8(\text{OH})_6$).

Chondrodite and clinohumite were observed in all subsolidus assemblages with Di + Grt + Amph + KMgF_3 , and there is a general progression upon increasing P and T from chondrodite to clinohumite to olivine in the amphibole-stable field. The fact that F-bearing chondrodite and clinohumite appear in these experiments, and that natural low-Ti, low-F humite-group minerals are rare strongly, suggests that F stabilizes them considerably more than OH.

Melt/Fluid Compositions

The compositions of melt and probably fluid (Table 3), manifested by glass and quench products (the intergrowth of glass and crystals or hydrous fluid – now lost or dehydrated – and crystals believed to have grown during the quench process), are somewhat difficult to evaluate in this study because 1) melt/fluid fractions are generally small, 2) thermal gradients led to compaction so liquids were only in equilibrium with touching solids, 3) quench products are difficult to analyze accurately,

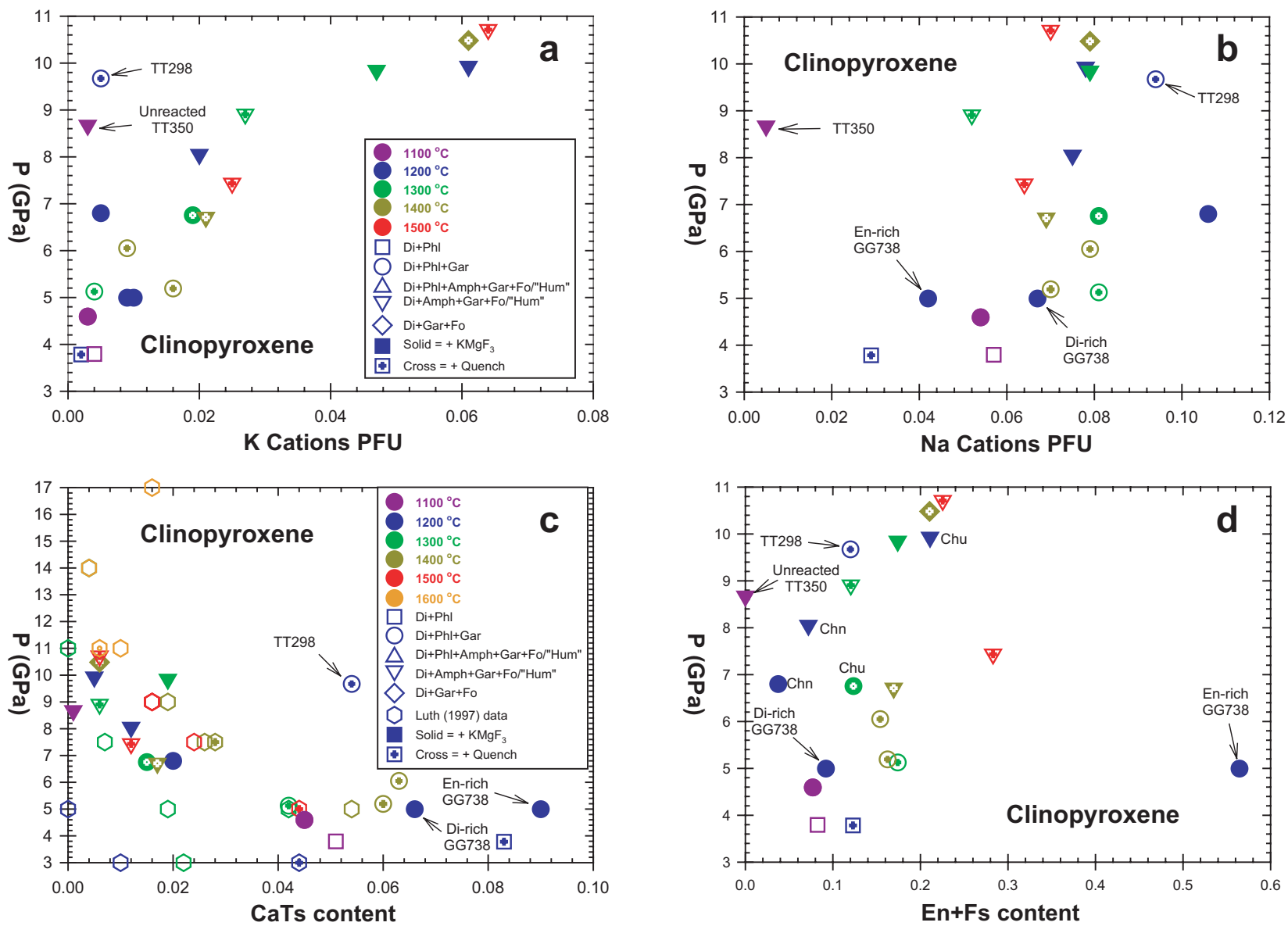


Figure 7. Scatter plots of aspects of clinopyroxene composition from experiments. a) K versus P; b) Na versus P; c) CaTs versus P; d) En+Fs versus P.

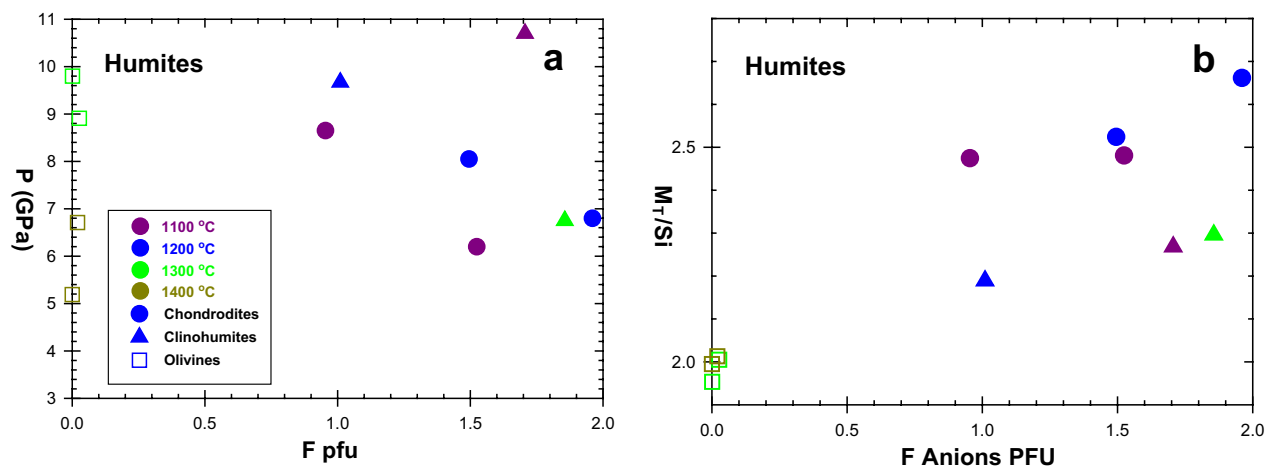


Figure 8. Scatter plots of aspects of chondrodite, clinohumite and olivine composition from experiments. a) F versus P; b) F versus octahedral metal cations (M_T).

and 4) the two-temperature experiments are not easily interpreted for melt composition. The latter aspect is the most daunting because examination of the compositional trends, with either initial T or final T as the actual temperature, shows that neither yields a reasonable pattern.

The compositions of small-fraction melts (or liquids) are both variable in major elements such as SiO_2 and CaO and significantly different from the melts reported from the experiments by Luth (1997). This suggests they are more “fluid” than melt. Luth only reported melts with melt fractions of ~20-40 or higher, so the lowest SiO_2 contents reported are ~45 wt% (original bulk content of ~49 wt%) as compared with low-fraction compositions here (Fig 9a,b – only experiments at lowest T at P and low Al_2O_3 are selected for internal consistency) with lowest SiO_2 content of ~12 wt% and highest ~38 wt% (bulk here is ~45 wt%). Separating K and Al in Fig. 9a, one can see the trend of an increase in SiO_2 and very low Al_2O_3 upon increasing pressure, demonstrating the sequestration of Al in garnet. K and F nearly covary with increases at constant T and rising P in the Phl field and the opposite occurs in the Kamph field; these variations may relate to F-bearing solids always containing K. There is an interesting contrast with the behavior of K and Al, which covary in Luth’s experiments. F always has greater concentration in the fluid/melt than the bulk. In Figure 9b, one can see that CaO decreases upon increasing P, MgO varies more irregularly, but then both values converge with the results of Luth at highest pressure (and temperature).

More generally there may be two trends in all of the melt/quench data: 1) the obvious effect of decreasing melt proportion upon increasing P at constant T (or T processing) which increases incompatible elements and de-

creases compatible elements in the melt, and 2) crystallization of Kamph drives the melt composition toward the bulk composition. As shown by Luth (1997) MgO behaves somewhat as an incompatible element, following K_2O and F in ranges below and above Kamph crystallization, but follows SiO_2 in the range of 7-9 GPa (Fig 9c). Stalder and Ulmer (2001) found that MgO strongly partitions into fluid while SiO_2 remains in solids; the low-T quenches here at lower pressures show a similar MgO enrichment over SiO_2 and thus may be indeed solute-rich fluids rather than melts.

Discussion

Compositions and geothermobarometers

Several of the experiments yielded the assemblage $\text{Opx} + \text{Cpx} + \text{Grt} \pm \text{Fo}$, including problematic TT298, which can be examined for consistency between experimental conditions and results of various geothermobarometers (Table 4). These include T [BKN], Opx-Cpx (two-pyroxene) thermometer, T [CaOpx], Ca in Opx thermometer, T [NaPx] Na partitioning between Opx and Cpx thermometer, and P [BKN] Al in Opx barometer (Brey and Kohler, 1990); T [KB] and P [KB], Ca partitioning between Cpx and Ol (Koehler and Brey, 1990); T [Wells], T [BM], and T [T], two-pyroxene thermometers (Wells, 1977; Bertrand and Mercier, 1985; and Taylor, 1998; respectively); and P [NG] and P [MG], Al in Opx barometers (Nickel and Green, 1985; MacGregor, 1974; respectively). The thermometers that yield T’s closest to experimental values for all three examples are the two-pyroxene thermometers T [BKN], T [BM], and T [T]. BB692 and BB705 yield barometric estimates that are low by 1 to 3 GPa. By comparison troubled TT298 with compositional trends (e.g. K and CaTs in Cpx or Si, Al and Na in Grt) that would suggest a pressure < 7 GPa

Table 3. Glass and quench compositions based on averaged, broad-beam microprobe analyses.

Exper.	TT320	BB438	GG738	TT298	GG746	BB361	GG524	GG748	TT286	TT270	BB709	BB709	BB705	BB702	GG733
# Anals	41	23	18	60	120	24	20	100	52	20	12	100	18	100	32
Gl or Q	Gl	Q	Q	Q	Q	Q	Q	Q	Q	Q	Gl	Q	Q	Q	Q
SiO ₂	36.67	16.40	43.93	12.10	11.51	17.06	18.35	39.49	33.17	23.31	43.66	42.38	31.01	38.19	33.87
TiO ₂	0.18	0.21	0.05	0.19	0.15	0.19	0.33	0.14	0.22	0.18	0.08	0.09	0.06	0.12	0.13
Al ₂ O ₃	9.75	1.77	12.24	1.59	1.73	1.32	1.27	9.04	4.83	1.80	5.48	5.25	1.30	2.56	2.63
MgO	21.17	17.30	26.10	24.61	23.08	23.77	15.61	18.40	20.99	26.58	24.76	23.24	24.80	21.28	24.68
CaO	15.26	10.96	3.74	17.78	18.03	9.18	2.27	9.88	9.98	9.60	8.07	8.34	5.27	8.24	6.48
FeO	0.87	0.54	0.04	0.73	0.64	0.45	0.95	0.48	0.87	0.74	0.84	0.82	0.31	0.75	0.76
BaO	0.21	3.02	0.26	1.42	1.59	2.46	2.02	0.51	0.83	1.91	0.50	0.47	1.97	0.75	0.90
Na ₂ O	1.95	2.25	0.34	2.93	2.28	2.28	0.58	1.29	1.61	1.05	0.97	0.71	0.67	1.34	1.01
K ₂ O	2.02	23.55	7.61	10.08	10.65	18.31	13.05	10.95	12.29	16.27	10.27	8.98	19.93	12.17	16.58
F	6.25	6.13	3.52	13.69	9.16	16.92	8.06	6.10	8.56	13.22	6.24	5.60	16.72	9.87	11.20
O=F	-2.63	-2.58	-1.48	-5.76	-3.86	-7.12	-3.39	-2.57	-3.61	-5.57	-2.63	-2.36	-7.04	-4.16	-4.72
Total	91.70	79.55	96.35	79.36	74.96	84.81	59.08	93.71	89.74	89.09	98.23	93.54	95.01	91.11	93.54
Cations per 6 oxygens															
Si	1.541	1.062	1.670	0.777	0.766	1.053	1.456	1.668	1.559	1.240	1.734	1.753	1.532	1.741	1.577
Ti	0.006	0.010	0.001	0.009	0.007	0.009	0.020	0.004	0.008	0.007	0.002	0.003	0.002	0.004	0.005
Al	0.483	0.136	0.549	0.120	0.135	0.096	0.119	0.450	0.268	0.113	0.256	0.256	0.076	0.137	0.144
Mg	1.326	1.671	1.480	2.355	2.289	2.186	1.847	1.159	1.471	2.109	1.466	1.433	1.826	1.446	1.713
Ca	0.687	0.761	0.152	1.223	1.285	0.607	0.193	0.447	0.503	0.547	0.343	0.370	0.279	0.403	0.323
Fe	0.031	0.029	0.001	0.039	0.035	0.023	0.063	0.017	0.034	0.033	0.028	0.029	0.013	0.028	0.030
Ba	0.003	0.077	0.004	0.036	0.041	0.059	0.063	0.008	0.015	0.040	0.008	0.008	0.038	0.013	0.016
Na	0.159	0.283	0.025	0.365	0.294	0.273	0.089	0.106	0.147	0.108	0.075	0.057	0.064	0.118	0.092
K	0.108	1.946	0.369	0.825	0.904	1.441	1.321	0.590	0.737	1.105	0.520	0.474	1.256	0.708	0.985
Total	4.345	5.974	4.251	5.750	5.758	5.748	5.170	4.450	4.741	5.302	4.433	4.382	5.087	4.599	4.884
F	0.830	1.255	0.423	2.779	1.927	3.302	2.023	0.815	1.273	2.226	0.783	0.733	2.613	1.423	1.649
Mg/Si	0.861	1.573	0.886	3.031	2.988	2.076	1.269	0.695	0.944	1.701	0.845	0.818	1.192	0.831	1.086

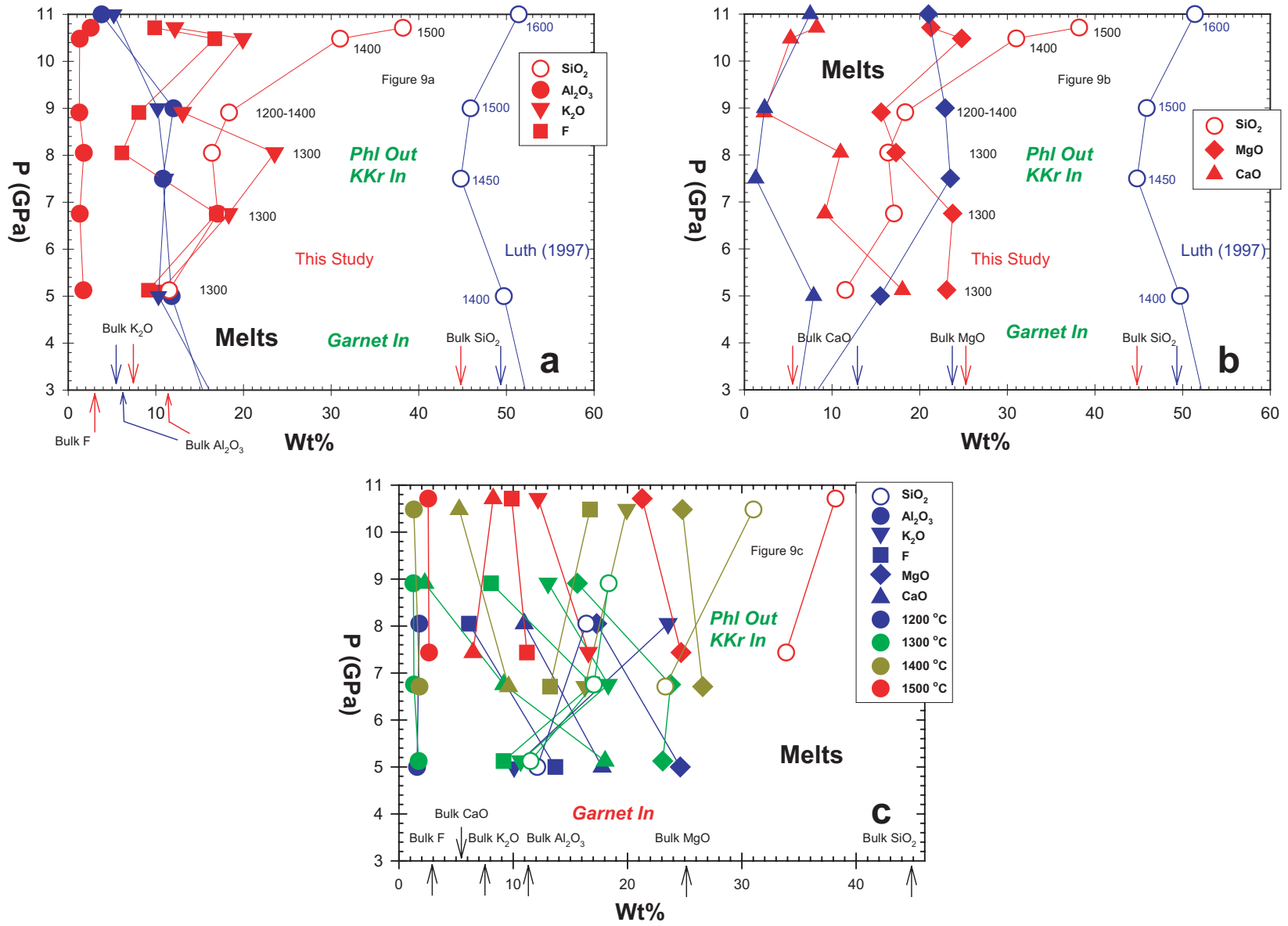


Figure 9. Scatter plots of melt/quench components versus P. a) and b) for lowest T at a particular P (see text); c) trends for particular T's at various P's.

Table 4. Geothermobarometers and experimental results¹.

Experiment	TT298	BB692	BB705
Exper. T (°C)	1200	1300	1400
Exper. P (GPa)	9.7	9.8	10.5
T [BKN]	1106	1367	1477
T [KB]	-	1513	-
T [CaOpx]	1062	1369	1307
Two-pyroxene Temperatures			
T [NaPx]	1090	1328	1147
T [Wells]	1004	1165	1256
T [BM]	1108	1355	1452
T [T]	1165	1328	1404
P [BKN]	8.0	6.9	8.2
P [KB]		6.1	
P [NG]	6.4	6.5	7.9
P [MG]	7.5	7.6	9.0

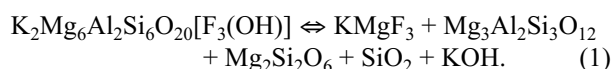
¹ Calculations were made with the Excel spreadsheet PTEXL2_2 by Andrei Girmis <girmis@jgem.ru> and Thomas Koehler.

yields a much higher calculated P. Obviously, extension of the experimental bases for barometers above 6 GPa is required.

The experiments do point to potential barometers at higher pressures. The K content of Cpx and Kamph are sensitive to P and may cross-correlate when they are the only K-bearing phases present. The trend and maximum K_{cpx} contents of ~6% (~1.3 wt% K₂O) at 10-11 GPa are much higher in my experiments than those in Konzett and Ulmer (1999) and are only approached by Luth (1997), whose experiments extended to 17 GPa; so the generally higher K content of the bulk composition here needs to be included in any parameterization. The content of Si, Al, and Na in Grt are sensitive to P even though Ca-Mg systematics are variable and slightly correlated with Si and Al.

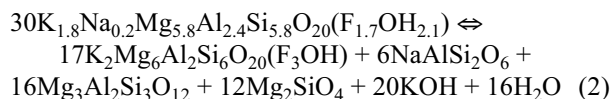
Reacting phlogopite and forming KMgF₃

Newly observed experimentally, KMgF₃ is undoubtedly the product of the breakdown of phlogopite, with the form of a reaction being something like:



This reaction, though written as univariant, would probably be continuous as the real phlogopite is a com-

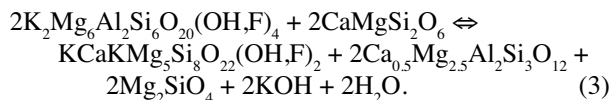
plex solid-solution. For example, F and OH should repartition, and F content in phlogopite, which goes to form KMgF₃, might be expected to decrease in coexisting phlogopite as the reaction progresses. On the contrary, F in Phl increases initially as P (and T) increases, but decreases just prior to Kamph formation. This result may reflect unobserved Kamph in a few experiments near 6 GPa (e.g. BB173, BB361) or the prominent effects of a possible garnet-forming reaction from “refining” the Phl solid solution into end-member Phl



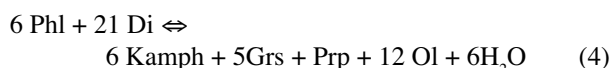
which also converts Na in Phl to jadeite. The point here is that “refining” Phl at high P would work in the directions observed in the experiments, driving up F content in Phl and creating garnet. Moreover, once KMgF₃ is formed from Phl at high P, there is no other phase that results from a subsolidus reaction with KMgF₃; it is thus stable through subsolidus conditions to at least 1400°C and >10 GPa.

Formation of potassic richterite, olivine, and humites

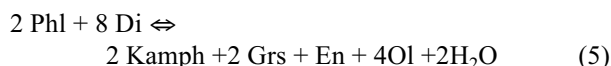
An important observation in these experiments is the presence of chondrodite and clinohumite at high pressure from a bulk composition that was low but not exceedingly depleted in silica (~45wt%). In the previous studies on this system, best summarized by Konzett and Ulmer (1999), the chemography for creating phases with Mg:Si > 1:1, such as olivine or the humites, is found in Grt + Kamph-forming reactions. So, first I will discuss those reactions and then the formation of humites. The basic Kamph-forming reaction, as proposed by Sudo and Tatsumi (1990) with a minor modification to show KOH instead of K₂O is:



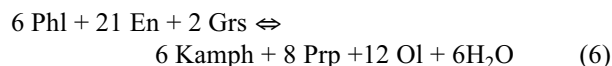
The more complete Schreinemaker’s analysis for KCMASH of Konzett and Ulmer (1999) yielded these equations which produce Kamph upon increasing P:



at lower T and



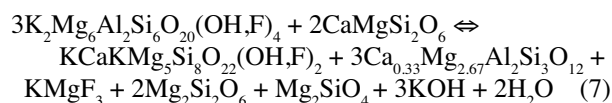
at higher T and



at higher T and P.

A couple of features stand out from these model reactions. First, reaction (3) yields garnet of approximately the composition observed in the experiments [$\text{Ca}/(\text{Ca}+\text{Mg})_{\text{Grt}} \approx 0.15$ for less zoned garnets] and consumes Phl and Cpx at the same rate, whereas reactions (4) and (5) produce excess grossular, which is not observed. Second, reactions (4) and (5) would consume all Cpx before Phl is consumed, whereas the reverse is observed, and reaction (6) would not be encountered in the experiments (see Fig. 10b of Konzett and Ulmer, 1999).

If the formation of KMgF_3 is taken into account in a simple additive way via the reaction

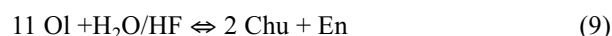


as an indication of how the phases react to yield both Kamph and KMgF_3 , then Phl will disappear prior to Cpx, as observed, and the garnet will be somewhat more magnesian than the value from equation (3) ($\text{Ca}/(\text{Ca}+\text{Mg}) = 0.167$), which is consistent with observed values for the less zoned garnets. Moreover, aspects of the compositions of Phl and Kamph – $\text{K}/(\text{K}+\text{Na})_{\text{Phl}} = 0.96$; $\text{K}/(\text{K}+\text{Na})_{\text{Kamph}} = 0.82$; and $\text{F}/(\text{F}+\text{OH})_{\text{Phl}} = 0.425$; $\text{F}/(\text{F}+\text{OH})_{\text{Kamph}} = 0.241\text{--}0.359$ (for sub-solidus runs w/o Phl) are consistent with the sharing of K+Na between Kamph, KMgF_3 , and Cpx, and F between Kamph and KMgF_3 , although F may also enter the aqueous fluid.

To form F-rich chondrodite, $(\text{Mg}_2\text{SiO}_4)_2 \cdot \text{Mg}(\text{F},\text{OH})_2$ and clinohumite, $(\text{Mg}_2\text{SiO}_4)_4 \cdot \text{Mg}(\text{F},\text{OH})_2$, reactions or conversions of the form



and



are required. Hence, the humites should coexist with both Grt and Opx. Although Opx was not found as a separate phase in humite-bearing experiments (Table 2), it is likely accounted in the Cpx compositions (Fig. 7d) except perhaps for those experiments at 1100°C for which accurate Cpx measurements were not possible. However, one other

possibility is the excess En (or silica) activity went into the fluid that would largely be in quench products. This may be evidenced by MgO behaving somewhat as an incompatible element in the quenches as noted above.

The multianvil experiments on a serpentinite starting composition $(\text{Mg}_3\text{Si}_2\text{O}_5(\text{OH})_4)$ by Stalder and Ulmer (2001) argue for relative MgO enrichment and silica depletion in the fluid, opposite to the suggestion above. These experiments (5–14 GPa; 800–1200°C) manifest silica enrichment (and H_2O depletion) in a central En-rich zone of the capsules, while fluid and hydrous phases in the periphery develop $\text{Mg}/\text{Si} > 2$ (that of olivine) driven by concentration of MgO in hydrous phases and fluid. Of the experiments here that yielded clinohumite or chondrodite, only two manifested a quench zone, both with $\text{Mg}/\text{Si} \leq 2$, and the solid assemblages with humites always contain the full mixture of hydrous and anhydrous phases. So greater SiO_2 in the quench is possible for these experiments. Perhaps the lower water content and higher F content here does not enable the mobility of MgO via hydration or fluid migration seen by Stalder and Ulmer (2001), which would also explain the generally restitic behavior of MgO in the experiments reported here.

High pressure synthesis and phase equilibrium experiments on clinohumite and chondrodite have been carried out in the MSH system by Yamamoto and Akimoto (1974, 1977), Kanzaki (1991), Luth (1995), Wunder (1998), and Pawley (2000), and only Stalder and Ulmer (2001) have introduced fluorine (0.1 wt%). In equilibrium stability experiments, particularly with excess H_2O or brucite $[\text{Mg}(\text{OH})_2]$, both humites have been shown to be stable over a broad range of P and T (2 to ~10 GPa and 600 to 1100°C), with indications that clinohumite is stable to lower P and to higher T than chondrodite. These humites break down to olivine + periclase + vapor above 1200°C and to Phase A, Phase E $[\text{Mg}_{2.3}\text{Si}_{1.25}\text{H}_{2.4}\text{O}_6]$ or Phase B $[\text{Mg}_{12}\text{Si}_4\text{O}_{19}(\text{OH})_2] \pm$ anhydrous Mg-silicates \pm fluid above 10–12 GPa below 1200°C, depending on bulk composition. Kanzaki (1991) and Luth (1995) carried out synthesis experiments and only produced clinohumite above 9 GPa, whereas Stalder and Ulmer (2001) found that F stabilized clinohumite to 4 GPa (the lowest pressure in their study) with an increasing F content in clinohumite upon decreasing pressure (from $\text{F}/(\text{F}+\text{OH})$ of <0.1 above 10 GPa to ~ 0.35 at 5 GPa). This trend is demonstrated in humites here, but here the relative increase is at much higher F content and is smaller as a proportion of the total univalent anions (see Fig. 8b). Chondrodite was only found by Stalder and Ulmer (2001) at 12 GPa and $\leq 950^\circ\text{C}$. Given the constraint of the olivine-forming reaction as the low-P limit for humite formation in the experiments here, clinohumite

stability is comparable to the broadest range from the previous experiments and chondrodite stability is consistent with reversed experiments but much broader than the synthesis experiments. As the experiments here are syntheses, F must be important to enhanced stability of the humites.

Natural occurrences of clinohumite + potassic richterite from enclaves in kimberlites have some similarities to the experimental assemblages. Taskayev and Ilupin (1991) described an intergrowth of the two minerals from the Kolletivnaya kimberlite pipe. The clinohumite, with Ti between 0.17 and 0.41 apfu and F between 0.7 and 0.85 apfu is similar to values here, even though a positive correlation of Ti and negative correlation of F with Fe (~0.65 apfu) cannot be evaluated in the experiments. Kamph contains ~0.92 K (~0.45 K/(K+Na)), ~7.8 Si, ~0.05 Al, and ~0.35 F apfu. Matsyuk et al. (1991) described a Kamph + Chu + ilmenite bearing dunite from the Slyudyanka pipe where the Ti and Fe content in clinohumite are higher, as may be expected with coexisting ilmenite (but still low for most mantle Ti-clinohumites which have > 2 wt% TiO₂ [~0.16 Ti apfu] – see Matsyuk et al., 1991), and F content is lower. Only one amphibole composition is given with 1.0 K (0.50 K/(K+Na)), 7.9 Si, and 0.03 Al but no F data. The lower K (and K/(K+Na)) and very low Al in K-rich richterites in the enclaves, compared to the experiments here, represent the much lower bulk K and Al contents in the enclaves and any once-coexisting liquid as well as likely lower P (e.g. no garnet). The closest experimental analogs are from Konzett et al. (1997) for a MARID-like (mica-amphibole-rutile-ilmenite-cpx) system in which similar low Al and (K/K+Na) are produced at ~2 GPa at T ≤ 1100°C. Although the above authors suggest both igneous and metasomatic parageneses at similar P and T, all the experimental results indicate a metasomatic (subsolvus open system) origin is required, particularly with the lack of cpx and mica in the enclaves.

The Significance and Behavior of Fluorine

With respect to fluorine, the new results here indicate that for some bulk compositions (such as Di + Phl) certain F+OH-bearing phases form at high P and T whereas the F-free, OH-bearing counterparts do not, specifically, clinohumite, chondrodite and KMgF₃. For other phases the effect of F on stability is less clear from these experiments. The inference for an enhanced stability for F-bearing mica (with rising T) is known and for amphibole is not yet sufficiently demonstrated. Otherwise, the stability fields of these are not shown to be changed relative to the inconsistent data from the F-free systems. F-content in Kamph and humites appears to decrease upon increasing P, but is affected by the coexisting KMgF₃, so

ultimate high-P stability is not yet known in the F-rich systems. What the data do suggest is where F enhances stability, whether at higher T or for varied bulk composition, there is also OH, so water retention should be enhanced as well.

As shown recently by Stalder and Ulmer (2001), preservation of humites – and water – in subducted slabs or metasomatized peridotite must be considered as probable; in particular even minor F content needs to be taken into account. Wunder (1998) dismissed clinohumite and chondrodite as mantle phases as being too Mg-rich, but both Stalder and Ulmer's and the experiments here show both that excessively Mg-rich compositions are not necessary and that fluid composition (and fluid transport) may play a crucial role for humite stability in the mantle. Indeed, the F-enriched phases may not be of great significance in average mantle, but metasomatism may enhance fluorine recycled from the crust in certain mantle regimes and in down going slabs. Moreover, like the apparent omnipresence of water (OH) in small amounts (but oceans of total content) in nominally anhydrous mantle minerals, minor F content may be more common in mantle olivine than presently perceived. However, preservation of F-rich phases in xenoliths or inclusions or minor F in olivine may be equally unlikely to permit its evaluation in mantle processes.

Edgar and Charbonneau (1991) have argued from evidence in certain F-bearing lamproites that F preferentially enters solids rather than liquids. While the results here do not directly support that inference, they do support persistence of F in high pressure minerals up to melting conditions. However, at least above 5 GPa and at concentrations as high as seen here, F is greater in coexisting fluid/melt than in amphibole or humite; KMgF₃ is the key to retaining higher F in solids. Perhaps a drier system would be a better test for some fundamental low-level limit for fluorine retention at these high pressures.

Acknowledgments

I am particularly grateful and indebted to Dave Walker for access to multianvil equipment and lunchtime bridge. The manuscript was improved by editor John Brady and through reviews by Jürgen Konzett, Bob Luth, and Dave Walker. I gratefully acknowledge the National Science Foundation (EAR-9314819 and EAR-9903203) for support of this research.

References Cited

- Bertrand, P., and Mercier, J.-C.C. (1985) The mutual solubility of coexisting ortho- and clinopyroxene: toward an absolute geothermometer for the natural system? *Earth and Planetary Science Letters*, 76, 109-122.
- Brey, G., and Köhler, T. (1990) Geothermobarometry in four-phase lherzolites II. New thermobarometers, and practical assessment of existing thermobarometers. *Journal of Petrology*, 31, 1353-1378.
- Deer, W.A., R.A. Howie, and J. Zussman (1982) *Humite Group In Rock-forming Minerals, Vol. 1A, Orthosilicates*. New York, Halsted Press, 379-417.
- Dymek, R.F., Boak, J.L., and Brothers, S.C. (1988) Titanian chondrodite- and titanian clinohumite-bearing metadunite from the 3800 Ma Isua supracrustal belt, West Greenland: Chemistry, petrology and origin. *American Mineralogist*, 73, 547-558.
- Edgar, A.D., and Charbonneau, H.E. (1991) Fluorine-bearing phases in lamproites. *Mineralogy and Petrology*, 44, 125-149.
- Edgar, A.D., and Vukadinovic, D. (1993) Potassium-rich clinopyroxene in the mantle: An experimental investigation of a K-rich lamproite up to 60 kbar. *Geochimica et Cosmochimica Acta*, 57, 5063-5072.
- Finger, L.W. (1972) The Uncertainty in the Calculated Ferric Iron Content of a Microprobe Analysis. *Year Book - Carnegie Institution of Washington*, 71, 600-603.
- Foley, S. (1991) High-pressure stability of fluor- and hydroxyl-endmembers of pargasite and K-richterite. *Geochimica et Cosmochimica Acta*, 55, 2689-2694.
- Gasparik, T. (1986) Experimental study of subsolidus phase relations and mixing properties of clinopyroxene in the silica-saturated system CaO-MgO-Al₂O₃-SiO₂. *American Mineralogist*, 71, 686-694.
- Harlow, G.E. (1996) Structure refinement of a natural K-rich diopside: The effect of potassium on the average structure. *American Mineralogist*, 81, 632-638.
- Harlow, G.E. (1997) K in clinopyroxene at high pressure and temperature: An experimental study. *American Mineralogist* 82, 259-269.
- Harlow, G.E. (1999) Interpretation of Kcpx and CaEs in Clinopyroxene from Diamond Inclusions and Mantle Samples. In Gurney, Gurney, Pascoe and Richardson, editors, *Proceedings of Seventh International Kimberlite Convention Volume I*, 321 - 331, Redroof Design, Cape Town.
- Harlow, G.E., and Veblen, D.R. (1991) Potassium in clinopyroxene inclusions in diamonds. *Science*, 251, 652-655.
- Inoue, T., Irifune, T., Yurimoto, H., and Miyagi, I. (1998) Decomposition of K-amphibole at high-pressure: implications for subduction zone volcanism. *Physics of the Earth and Planetary Interiors*, 107, 221-231.
- Irifune, T., Ringwood, A.E., and Hibberson, W.O. (1994) Subduction of continental crust and terrigenous and pelagic sediments: an experimental study. *Earth and Planetary Science Letters*, 77, 351-368.
- Kanzaki, M. (1991) Stability of hydrous magnesium silicates in the mantle transition zone. *Physics of the Earth and Planetary Interiors*, 66, 307-312.
- Koehler, T., and Brey, G.P. (1990) Calcium exchange between olivine and clinopyroxene calibrated as a geothermobarometer for natural peridotites from 2 to 60 kb with applications. *Geochimica et Cosmochimica Acta*, 54, 2375-2388.
- Konzett, J., and Fei, Y. (2000) Transport and storage of potassium in the Earth's upper mantle and transition zone: an experimental study to 23 GPa in simplified and natural bulk compositions. *Journal of Petrology*, 41, 583-603.
- Konzett, J., Sweeney, R.J., Thompson, A.B., and Ulmer, P. (1997) Potassium amphibole stability in the upper mantle: an experimental study in a peralkaline KNCMASH system to 8.5 GPa. *Journal of Petrology*, 38, 537-568.
- Konzett, J., and Ulmer, P. (1999) The stability of hydrous potassic phases in lherzolitic mantle - an experimental study to 9.5 GPa in simplified and natural bulk compositions. *Journal of Petrology*, 40, 629-652.
- Kretz, R. (1983) Symbols for rock-forming minerals. *American Mineralogist*, 68, 277-279.
- Luth, R.W. (1995) Is phase A relevant to the Earth's mantle? *Geochimica et Cosmochimica Acta*, 59, 679-682.
- Luth, R.W. (1997) Experimental study of the system phlogopite-diopside from 3.5 to 17 GPa. *American Mineralogist*, 82, 1198-1209.
- MacGregor, I.D. (1974) The system MgO-Al₂O₃-SiO₂: solubility of Al₂O₃ in enstatite for spinel and garnet peridotite compositions. *American Mineralogist*, 59, 110-119.
- Massonne, H.J. (1992) Evidence for low-temperature ultrapotassic siliceous fluids in subduction zone environments from experiments in the system

- K_2O - MgO - Al_2O_3 - SiO_2 - H_2O (KMASH). *Lithos*, 28, 21-434.
- Matsyuk, S.S., Vishnevskii, A.A., Cherenkova, A.F., and Egorova, L.N. (1991) K-richterite-bearing ilmenite-clinohumite dunite; a new variety. *Soviet Geology and Geophysics*, 32/12, 64-70.
- Mitchell, R.H. (1995) Melting experiments on a sanidine phlogopite lamproite at 4-7 GPa and their bearing on the sources of lamproite magmas. *Journal of Petrology*, 36, 1455-1474.
- Nickel, K.G., and Green, D.H. (1985) Empirical geothermobarometry for garnet peridotites and implications for the nature of the lithosphere, kimberlites and diamonds, *Earth and Planetary Science Letters*, 73, 158-170.
- Pawley, A. (2000) Stability of clinohumite in the system MgO - SiO_2 - H_2O . *Contributions to Mineralogy and Petrology*, 138, 284-291.
- Pouchou, J.L. and Pichoir, F., (1991) Quantitative analysis of homogenous or stratified microvolumes applying the model "PAP". In Heinrich, K.F.J., and Newbury, D.E. Eds., *Electron Probe Quantitation*, 31-75, Plenum Press, New York.
- Ribbe, P.H. (1980) The humite series and Mn-analogs. In Ribbe, P.H., Ed., *Orthosilicates, Reviews in Mineralogy*, 5, 231-274.
- Satish-Kumar, M., and Niimi, N. (1998) Fluorine-rich clinohumite from Ambasamudram marbles, Southern India: mineralogical and preliminary FTIR spectroscopic characterization. *Mineralogical Magazine* 62, 509-519.
- Schmidt, M.W. (1996) Experimental constraints on recycling of potassium from subducted oceanic crust. *Science*, 272, 1927-1930.
- Stalder, R. and Ulmer, P. (2001) Phase relations of a serpentine composition between 5 and 14 GPa: significance of clinohumite and phase E as water carriers into the transition zone. *Contributions to Mineralogy and Petrology*, 140, 670-679.
- Sudo, A. and Tatsumi, Y. (1990) Phlogopite and K-amphibole in the upper mantle: Implication for magma genesis in subduction zones. *Geophysical Research Letters*, 17, 29-32.
- Taskayev, V.I., and Ilupin, I.P. (1991) Clinohumite associated with K-richterite in the Kollektivnaya kimberlite pipe. *Doklady Akademii Nauk SSSR* 310/3, 683-686. (English translation: *Akademi Nauk: Transactions of the USSR Academy of Sciences: Earth Science Section*, 310, 153-156.)
- Taylor, W.R. (1998) An experimental test of some geothermometer and geobarometer formulations for upper mantle peridotites with application to the thermobarometry of fertile lherzolite and garnet websterite, *Neues Jahrbuch für Mineralogie. Abhandlungen*, 172, 381-408.
- Thibault, Y. (1993) The role of pressure and fluorine content in the distribution of K, Na, and Al in the upper mantle. *EOS Transactions, American Geophysical Union*, 74, 321.
- Trønnes, R.G. (1990) Low-Al, high-K amphiboles in subducted lithosphere from 200-400 Km depth: experimental evidence. *EOS Transactions*, 71, 1587.
- Tsuruta, K., and Takahashi, E. (1998) Melting study of an alkali basalt JB-1 up to 12.5 GPa: behavior of potassium in the deep mantle. *Physics of Earth and Planetary Interiors*, 107, 119-130.
- Wang, W., and Takahashi, E. (1999) Subsolidus and melting experiments of a K-rich basaltic composition to 27 GPa: Implication for the behavior of potassium in the mantle. *American Mineralogist*, 84, 357-361.
- Wells, P.R.A. (1977) Pyroxene thermometry in simple and complex systems. *Contributions to Mineralogy and Petrology*, 62, 129-139.
- Wunder, B. (1998) Equilibrium experiments in the system MgO - SiO_2 - H_2O (MSH): stability fields of clinohumite-OH [$Mg_9Si_4O_{16}(OH)_2$], chondrodite-OH [$Mg_5Si_2O_8(OH)_2$] and phase A [$Mg_7Si_2O_8(OH)_6$]. *Contributions to Mineralogy and Petrology*, 132, 111-120.
- Yagi, A., Suzuki, T., and Akaogi, M. (1994) High pressure transition in the system $KAlSi_3O_8$ - $NaAlSi_3O_8$. *Physics and Chemistry of Minerals*, 21, 12-17.
- Yamamoto, K., and Akimoto, S. (1974) High pressure and high temperature investigations in the system MgO - SiO_2 - H_2O . *Journal of Solid State Chemistry*, 9, 187-195.
- Yamamoto, K., and Akimoto, S. (1977) The system MgO - SiO_2 - H_2O at high pressures and temperatures. Stability field of hydroxyl-chondrodite, hydroxyl-clinohumite and 10Å-phase. *American Journal of Science*, 277, 288-312.
- Yang, H., Konzett, J., Prewitt, C.T., and Fei, Y. (1999) Single-crystal structure refinement of synthetic M^4K -substituted potassic richterite, $K(KCa)Mg_5Si_8O_{22}(OH)_2$. *American Mineralogist*, 84, 681-684.
- Zhao, Y., Weidner, D.J., Liu, X., Ko, J., Vaughan, M.T., Pacalo, R.E.G., Wang, Y., and Yeganeh-Haeri, A. (1990) High P-T X-ray study of $NaMgF_3$ and $KMgF_3$ perovskites. *Eos Transactions*, 71, 1610.

Table A1. Microprobe analyses of KMgF_3 in experiments.

Exper.	BB438	GG765	BB692	TT270	BB705
# Anals.	6	5	8	8	3
Si	0.00	0.00	0.00	0.00	0.01
Fe	0.01	0.01	0.01	0.02	0.02
Mg	20.15	20.75	20.35	20.41	20.93
Ca	0.03	0.00	0.00	0.00	0.00
Ba	0.14	0.19	0.24	0.09	0.12
K	31.63	31.91	31.93	32.13	31.97
Na	0.17	0.03	0.05	0.06	0.16
F	46.10	46.43	45.86	46.57	46.49
O	1.82	0.46	1.44	1.08	1.65
Total	100.04	99.79	99.88	100.35	101.34
Normalized Total Atoms					
Si	0.000	0.000	0.000	0.000	0.000
Fe	0.000	0.000	0.000	0.000	0.000
Mg	0.990	1.030	1.006	1.003	1.016
Ca	0.001	0.000	0.000	0.000	0.000
Ba	0.001	0.002	0.002	0.001	0.001
K	0.966	0.984	0.981	0.982	0.965
Na	0.009	0.002	0.003	0.003	0.008
F	2.898	2.948	2.900	2.930	2.887
O	0.135	0.034	0.108	0.081	0.121
Total	5.000	5.000	5.000	5.000	5.000

Table A2. Microprobe analyses of phlogopite in experiments.

Exper.	TT346	TT321	TT352	TT320	GG738	BB173	GG746	BB361	GG748	TT286
# Anals.	26	27	6	28	19	24	21	13	1	17
SiO ₂	41.13	42.28	43.70	41.88	43.47	42.76	43.09	44.18	43.56	43.25
TiO ₂	0.07	0.05	0.03	0.04	0.06	0.02	0.08	0.05	0.07	0.06
Al ₂ O ₃	13.50	13.68	10.77	13.56	12.43	11.70	11.99	10.97	12.35	11.63
Fe ₂ O ₃	0.00	0.00	0.00	0.00	0.00	0.00	0.00	0.04	0.00	0.00
FeO	0.37	0.25	0.35	0.10	0.01	0.43	0.32	0.45	0.25	0.41
MgO	27.35	27.26	26.81	27.64	27.28	27.57	27.49	27.95	26.54	27.44
CaO	0.05	0.12	0.11	0.06	0.05	0.06	0.05	0.11	0.23	0.01
BaO	0.40	0.46	0.29	0.52	0.35	0.36	0.26	0.15	0.62	0.33
Na ₂ O	0.62	0.45	0.14	0.29	0.11	0.15	0.15	0.21	0.08	0.13
K ₂ O	9.87	9.96	10.38	10.38	10.81	10.52	10.79	10.71	10.84	10.83
F	4.82	4.46	3.73	4.78	4.84	3.38	5.40	3.81	5.34	5.16
H ₂ O*	1.93	2.16	2.42	2.00	1.98	2.62	1.69	2.48	1.73	1.79
O=F	-2.03	-1.88	-1.57	-2.01	-2.04	-1.42	-2.28	-1.60	-2.25	-2.17
Total	98.06	99.25	97.15	99.24	99.36	98.14	99.03	99.50	99.36	98.86
Si	5.860	5.934	6.255	5.897	6.095	6.079	6.080	6.186	6.131	6.117
^[4] Al	2.140	2.066	1.745	2.103	1.905	1.921	1.920	1.809	1.869	1.883
^[4] Fe ⁺³	0.000	0.000	0.000	0.000	0.000	0.000	0.000	0.004	0.000	0.000
Sum T	8.000	8.000	8.000	8.000	8.000	8.000	8.000	8.000	8.000	8.000
Ti	0.007	0.005	0.003	0.004	0.006	0.002	0.008	0.006	0.008	0.006
^[6] Al	0.126	0.197	0.071	0.147	0.150	0.039	0.074	0.000	0.179	0.054
Fe ³⁺	0.000	0.000	0.000	0.000	0.000	0.000	0.000	0.000	0.000	0.000
Fe ²⁺	0.044	0.029	0.042	0.012	0.002	0.051	0.038	0.053	0.029	0.048
Mg	5.810	5.703	5.719	5.801	5.704	5.843	5.782	5.833	5.569	5.785
Ca	0.007	0.018	0.017	0.010	0.008	0.009	0.008	0.017	0.035	0.001
Ba	0.023	0.025	0.017	0.028	0.019	0.020	0.015	0.008	0.034	0.018
Na	0.171	0.122	0.037	0.081	0.030	0.040	0.040	0.057	0.020	0.035
K	1.793	1.783	1.894	1.864	1.933	1.909	1.943	1.913	1.947	1.954
Total	15.982	15.882	15.800	15.946	15.853	15.913	15.907	15.886	15.821	15.903
F	2.170	1.978	1.689	2.127	2.148	1.518	2.412	1.688	2.378	2.307
OH*	1.830	2.022	2.311	1.873	1.852	2.482	1.588	2.312	1.622	1.693
K/(K+Na)	0.913	0.936	0.981	0.959	0.984	0.979	0.980	0.971	0.990	0.982

* Formula is calculated with 20 O + 4(F+OH); OH is calculated to fill univalent anion site, and H₂O is back calculated from the conversion of wt percent values to cations.

Table A3. Microprobe analyses of amphibole in experiments.

Exper	TT350	BB438	GG765	GG524	BB692	TT270	GG733	BB702	TT353	TT352
# Anals.	11	9	11	17	39	39	11	5	11	8
SiO ₂	53.53	53.75	55.27	53.48	54.71	53.62	53.98	53.92	52.95	52.35
TiO ₂	0.01	0.03	0.03	0.03	0.03	0.03	0.01	0.04	0.02	0.03
Al ₂ O ₃	1.32	2.23	1.15	1.86	0.95	2.52	2.26	1.85	1.79	2.90
Fe ₂ O ₃	0.25	0.20	0.25	0.06	0.22	0.17	0.27	0.53	0.27	0.04
FeO	0.00	0.00	0.00	0.16	0.00	0.00	0.00	0.00	0.00	0.11
MgO	22.45	23.73	23.42	22.92	23.59	23.64	23.69	22.96	22.53	22.56
CaO	6.82	7.84	6.94	7.55	6.36	7.82	7.58	6.81	6.40	7.74
BaO	0.08	0.00	0.09	0.05	0.09	0.04	0.03	0.10	0.08	0.04
Na ₂ O	1.39	1.39	1.22	1.10	1.15	1.14	1.07	1.15	1.23	2.12
K ₂ O	8.88	7.70	8.74	7.93	9.19	7.78	8.10	9.96	8.45	6.11
F	1.19	1.57	1.07	1.83	1.82	2.73	2.75	2.01	1.55	2.60
H ₂ O*	1.50	1.37	1.60	1.20	1.23	0.81	0.81	1.15	1.31	0.83
O=F	-0.50	-0.66	-0.45	-0.77	-0.77	-1.15	-1.16	-0.85	-0.65	-1.09
Total	96.91	99.17	99.32	97.40	98.57	99.15	99.39	99.62	95.94	96.32
Si	7.778	7.627	7.844	7.743	7.839	7.624	7.660	7.688	7.775	7.626
⁴ Al	0.222	0.373	0.156	0.257	0.161	0.376	0.340	0.310	0.225	0.374
⁶ Al	0.004	0.000	0.037	0.060	0.000	0.045	0.037	0.000	0.086	0.124
Ti	0.001	0.004	0.003	0.003	0.003	0.003	0.002	0.004	0.002	0.003
Fe ³⁺	0.027	0.021	0.027	0.006	0.024	0.018	0.029	0.057	0.030	0.004
Fe ²⁺	0.000	0.000	0.000	0.020	0.000	0.000	0.000	0.000	0.000	0.014
Mg	4.862	5.020	4.954	4.947	5.040	5.010	5.010	4.879	4.933	4.899
Sum M1,2,3	4.894	5.044	5.020	5.035	5.067	5.076	5.078	4.940	5.051	5.044
Excess to M4	0.000	0.044	0.020	0.035	0.067	0.076	0.078	0.000	0.051	0.044
Ca	1.061	1.193	1.055	1.170	0.977	1.192	1.152	1.040	1.007	1.208
Na	0.391	0.383	0.335	0.309	0.319	0.315	0.295	0.318	0.349	0.599
K	0.548	0.380	0.590	0.486	0.637	0.417	0.475	0.642	0.593	0.149
Sum M4	2.000	2.000	2.000	2.000	2.000	2.000	2.000	2.000	2.000	2.000
K	1.097	1.013	0.992	0.980	1.041	0.994	0.990	1.169	0.990	0.987
Sum A	1.097	1.013	0.992	0.980	1.041	0.994	0.990	1.169	0.990	0.987
Total	15.992	16.013	15.992	15.980	16.041	15.994	15.990	16.108	15.990	15.987
F	0.548	0.706	0.481	0.837	0.825	1.229	1.232	0.908	0.718	1.198
OH*	1.452	1.294	1.519	1.163	1.175	0.771	0.768	1.092	1.282	0.802
K/(K+Na)	0.808	0.784	0.825	0.826	0.840	0.818	0.833	0.851	0.819	0.655

* Formula is calculated with 22 O + 2(F+OH); OH is calculated to fill univalent anion site, and H₂O is back calculated from the conversion of wt percent values to cations.

Table A4. Microprobe analyses of garnet in experiments.

Exper.	TT352	TT350 lo-Ca	TT350 hi-Ca	TT353	GG738	BB173	BB438	TT298	GG765	GG746	BB361
# Anals.	2	1	1	8	18	14	13	14	7	24	15
SiO ₂	44.37	45.23	43.77	44.14	45.13	43.60	44.63	43.24	44.75	44.14	44.10
TiO ₂	0.14	0.08	0.13	0.12	0.05	0.13	0.10	0.10	0.12	0.06	0.14
Al ₂ O ₃	23.56	21.45	20.57	20.07	22.92	23.51	23.17	23.61	22.66	24.18	22.91
Fe ₂ O ₃	0.16	1.30	1.58	1.26	0.04	1.35	0.76	2.02	0.95	0.40	0.95
FeO	0.24	0.00	0.00	0.00	0.00	0.00	0.00	0.00	0.00	0.00	0.00
MgO	24.04	25.37	23.28	25.26	27.28	23.42	25.30	24.20	25.39	25.29	25.25
CaO	6.81	4.94	9.05	4.91	4.97	8.36	6.28	7.13	5.89	6.38	6.26
BaO	0.00	0.01	0.05	0.03	0.01	0.02	0.00	0.01	0.02	0.01	0.01
Na ₂ O	0.09	0.12	0.11	0.24	0.02	0.07	0.10	0.04	0.14	0.03	0.07
K ₂ O	0.04	0.10	0.13	0.97	0.01	0.03	0.02	0.01	0.19	0.02	0.04
F	0.00	0.00	0.00	0.58	0.02	0.10	0.00	0.00	0.00	0.01	0.00
O=F	0.00	0.00	0.00	-0.24	-0.01	-0.04	0.00	0.00	0.00	-0.01	0.00
Total	99.45	98.60	98.67	97.34	100.44	100.55	100.36	100.36	100.11	100.51	99.73
Cations per 24 oxygens											
⁴ Si	6.000	6.000	6.000	6.000	6.000	5.998	6.000	5.951	6.000	6.000	6.000
⁴ Al	0.000	0.000	0.000	0.000	0.000	0.002	0.000	0.049	0.000	0.000	0.000
Sum T	6.000	6.000	6.000	6.000	6.000	6.000	6.000	6.000	6.000	6.000	6.000
⁶ Si	0.112	0.265	0.161	0.263	0.122	0.000	0.093	0.000	0.129	0.014	0.067
Ti	0.015	0.008	0.014	0.013	0.005	0.014	0.010	0.010	0.012	0.007	0.014
⁶ Al	3.825	3.502	3.412	3.356	3.664	3.811	3.728	3.780	3.658	3.883	3.715
Fe ³⁺	0.016	0.135	0.167	0.134	0.004	0.139	0.078	0.209	0.098	0.041	0.099
Fe ²⁺	0.028	0.000	0.000	0.000	0.000	0.000	0.000	0.000	0.000	0.000	0.000
Mg	4.937	5.238	4.885	5.343	5.517	4.803	5.150	4.964	5.183	5.136	5.180
Ca	1.006	0.734	1.365	0.746	0.722	1.232	0.918	1.051	0.864	0.932	0.922
Na	0.023	0.032	0.030	0.069	0.005	0.018	0.027	0.011	0.038	0.007	0.020
K	0.007	0.018	0.023	0.175	0.002	0.005	0.003	0.002	0.034	0.004	0.007
Total	15.968	15.932	16.058	16.099	16.041	16.022	16.009	16.027	16.016	16.023	16.024
F	0.000	0.000	0.000	0.260	0.009	0.045	0.002	0.000	0.000	0.006	0.001

Table A4 (continued). Microprobe analyses of garnet in experiments.

Exper.	GG524	GG524	BB692	GG748	TT286	TT270	BB709	BB705	GG733	BB702
	Lo-Ca	hi-Ca								
# Anals.	10	8	9	24	14	21	39	9	13	22
SiO ₂	45.51	44.18	46.25	44.71	44.21	44.48	45.51	47.00	45.24	47.63
TiO ₂	0.06	0.11	0.13	0.03	0.05	0.08	0.03	0.03	0.06	0.03
Al ₂ O ₃	21.92	22.21	21.01	24.00	23.48	22.98	22.00	20.62	22.70	19.50
Fe ₂ O ₃	0.58	0.99	0.89	0.04	0.67	0.47	0.52	0.53	0.81	0.77
FeO	0.00	0.00	0.00	0.00	0.00	0.00	0.00	0.00	0.00	0.00
MgO	28.82	25.49	26.29	27.25	24.98	26.27	27.02	27.91	27.46	28.35
CaO	2.25	5.45	5.56	3.90	6.63	5.29	4.28	4.72	3.97	4.58
BaO	0.01	0.05	0.02	0.00	0.01	0.01	0.01	0.01	0.01	0.00
Na ₂ O	0.06	0.06	0.16	0.02	0.04	0.05	0.06	0.15	0.06	0.17
K ₂ O	0.02	0.02	0.08	0.28	0.01	0.08	0.01	0.10	0.03	0.32
F	0.00	0.00	0.01	0.05	0.00	0.01	0.00	0.00	0.01	0.03
O=F	0.00	0.00	0.00	-0.02	0.00	0.00	0.00	0.00	0.00	-0.01
Total	99.24	98.56	100.39	100.27	100.08	99.72	99.44	101.05	100.35	101.38
Cations per 24 oxygens										
Si	6.000	6.000	6.000	6.000	6.000	6.000	6.000	6.000	6.000	6.000
^[4] Al	0.000	0.000	0.000	0.000	0.000	0.000	0.000	0.000	0.000	0.000
Sum T	6.000	6.000	6.000	6.000	6.000	6.000	6.000	6.000	6.000	6.000
^[6] Si	0.206	0.135	0.300	0.063	0.058	0.093	0.225	0.338	0.138	0.415
Ti	0.007	0.011	0.013	0.003	0.005	0.008	0.003	0.003	0.006	0.003
^[6] Al	3.523	3.635	3.373	3.837	3.792	3.711	3.545	3.277	3.630	3.096
Fe ³⁺	0.060	0.103	0.091	0.004	0.069	0.049	0.054	0.053	0.083	0.078
Fe ²⁺	0.000	0.000	0.000	0.000	0.000	0.000	0.000	0.000	0.000	0.000
Mg	5.860	5.276	5.338	5.511	5.102	5.366	5.509	5.611	5.554	5.692
Ca	0.329	0.811	0.812	0.567	0.974	0.776	0.627	0.682	0.577	0.661
Na	0.016	0.016	0.042	0.006	0.010	0.014	0.016	0.038	0.016	0.046
K	0.003	0.003	0.014	0.049	0.003	0.013	0.002	0.017	0.006	0.054
Total	16.005	15.992	15.982	16.040	16.013	16.032	15.981	16.020	16.010	16.045
F	0.002	0.002	0.003	0.020	0.001	0.003	0.002	0.000	0.004	0.012

Table A5. Microprobe analyses of pyroxenes in experiments.

Exper.	TT346	TT321	TT350	TT320	GG738	GG738	GG738	BB173	BB438	TT298	TT298	GG765	GG746
# Anals.	8	7	5	10	19	14	3	8	16	29	1	14	23
Phase	Cpx	Cpx	Cpx	Cpx	Cpx	Cpx	Opx ¹	Cpx	Cpx	Cpx	Opx	Cpx	Cpx
SiO ₂	53.92	54.37	54.05	53.58	54.35	55.44	55.12	55.04	55.33	54.04	58.07	56.20	55.18
TiO ₂	0.05	0.03	0.04	0.03	0.04	0.02	0.02	0.04	0.03	0.04	0.04	0.01	0.02
Al ₂ O ₃	3.16	3.00	0.06	4.01	4.87	5.64	8.85	2.82	2.28	3.73	0.24	2.75	3.80
Fe ₂ O ₃	0.23	0.08	0.11	0.38	0.06	0.02	0.00	0.63	0.30	0.82	0.23	0.60	0.29
FeO	0.00	0.00	0.00	0.00	0.00	0.01	0.03	0.00	0.00	0.00	0.00	0.00	0.00
MgO	18.32	18.47	18.25	19.19	17.96	27.73	33.74	17.42	18.24	18.42	40.50	20.41	19.87
CaO	22.58	22.90	25.60	22.48	21.93	10.42	2.90	21.85	21.97	20.84	0.53	17.42	19.61
BaO	0.01	0.01	0.01	0.01	0.01	0.01	0.01	0.00	0.00	0.01	0.04	0.00	0.01
Na ₂ O	0.81	0.78	0.08	0.42	0.97	0.63	0.22	1.57	1.08	1.35	0.08	1.14	1.18
K ₂ O	0.09	0.08	0.47	0.05	0.23	0.20	0.05	0.12	0.43	0.11	0.06	1.35	0.09
F	0.07	0.08	0.07	0.05	0.11	0.08	0.05	0.04	0.04	0.03	0.00	0.01	0.05
O=F	-0.03	-0.03	-0.03	-0.02	-0.05	-0.03	-0.02	-0.02	-0.02	-0.01	0.00	-0.01	-0.02
Total	99.23	99.76	98.70	100.18	100.48	100.15	100.96	99.52	99.69	99.37	99.79	99.89	100.09
Cations per 6 oxygens													
Si	1.947	1.953	1.985	1.915	1.932	1.910	1.842	1.980	1.986	1.944	1.958	1.995	1.956
^[4] Al	0.053	0.047	0.003	0.085	0.068	0.090	0.158	0.020	0.014	0.056	0.009	0.005	0.044
Sum T	2.000	2.000	1.987	2.000	2.000	2.000	2.000	2.000	2.000	2.000	1.967	2.000	2.000
Ti	0.001	0.001	0.001	0.001	0.001	0.000	0.000	0.001	0.001	0.001	0.001	0.000	0.001
^[6] Al	0.082	0.080	0.000	0.084	0.136	0.139	0.190	0.099	0.083	0.102	0.000	0.110	0.115
Fe ³⁺	0.006	0.002	0.003	0.010	0.002	0.001	0.000	0.017	0.008	0.022	0.006	0.016	0.008
Fe ²⁺	0.000	0.000	0.000	0.000	0.000	0.000	0.001	0.000	0.000	0.000	0.000	0.000	0.000
Mg	0.987	0.989	0.999	1.023	0.952	1.424	1.680	0.934	0.976	0.988	2.036	1.080	1.050
Ca	0.874	0.881	1.007	0.861	0.835	0.385	0.104	0.842	0.845	0.803	0.019	0.663	0.745
Na	0.057	0.054	0.005	0.029	0.067	0.042	0.014	0.110	0.075	0.094	0.005	0.078	0.081
K	0.004	0.003	0.022	0.002	0.010	0.009	0.002	0.006	0.020	0.005	0.002	0.061	0.004
Ba	0.000	0.000	0.000	0.000	0.000	0.000	0.000	0.000	0.000	0.000	0.001	0.000	0.000
Total	4.012	4.011	4.025	4.010	4.003	4.000	3.992	4.009	4.008	4.015	4.037	4.009	4.003
F	0.008	0.009	0.008	0.005	0.013	0.008	0.005	0.005	0.004	0.004	0.000	0.001	0.005

¹Opx considered to be a quench product.

Table A5 (continued). Microprobe analyses of pyroxenes in experiments.

Exper.	BB361	GG524	BB692	BB692	GG748	GG748	TT286	TT270	BB705	BB705	GG733	GG733	BB702
# Anals.	18	19	15	8	15	5	14	9	15	7	12	12	15
Phase	Cpx	Cpx	Cpx	Opx	Cpx	Opx ¹	Cpx	Cpx	Cpx	Opx	Cpx	Cpx	Cpx
SiO ₂	55.72	55.43	55.56	59.03	54.46	56.43	54.31	55.82	56.19	59.70	56.43	56.43	56.31
TiO ₂	0.03	0.01	0.04	0.01	0.02	0.01	0.02	0.02	0.01	0.01	0.01	0.01	0.02
Al ₂ O ₃	2.62	1.77	2.51	0.37	4.50	5.34	4.78	2.48	2.74	0.24	2.22	2.22	2.70
Fe ₂ O ₃	0.24	0.29	0.46	0.26	0.10	0.07	0.25	0.13	0.61	0.20	0.45	0.45	0.59
FeO	0.00	0.00	0.00	0.00	0.00	0.00	0.00	0.00	0.00	0.10	0.00	0.00	0.00
MgO	19.23	19.40	20.05	39.13	19.36	35.51	18.97	20.32	20.42	39.24	22.65	22.65	20.86
CaO	20.69	20.90	19.30	0.72	19.96	2.54	20.01	19.84	17.48	0.52	16.82	16.82	17.32
BaO	0.01	0.02	0.03	0.02	0.00	0.00	0.01	0.00	0.00	0.01	0.01	0.01	0.01
Na ₂ O	1.17	0.74	1.14	0.11	1.02	0.17	1.14	1.00	1.15	0.06	0.94	0.94	1.02
K ₂ O	0.42	0.58	1.04	0.17	0.51	0.16	0.20	0.47	1.34	0.13	0.56	0.56	1.42
F	0.06	0.01	0.00	0.00	0.17	-	0.09	0.05	0.01	0.01	0.04	0.04	0.04
O=F	-0.03	0.00	0.00	0.00	-0.07	-	-0.04	-0.02	0.00	0.00	-0.01	-0.01	-0.02
Total	100.17	99.15	100.13	99.82	100.03	100.24	99.75	100.11	99.94	100.23	100.09	100.09	100.27
Cations per 6 oxygens													
Si	1.983	1.994	1.979	1.986	1.938	1.899	1.935	1.981	1.994	1.997	1.988	1.988	1.992
^[4] Al	0.017	0.006	0.021	0.014	0.062	0.101	0.065	0.019	0.006	0.003	0.012	0.012	0.008
Sum T	2.000	2.000	2.000	2.000	2.000	2.000	2.000	2.000	2.000	2.000	2.000	2.000	2.000
Ti	0.001	0.000	0.001	0.000	0.001	0.000	0.001	0.001	0.000	0.000	0.000	0.000	0.001
^[6] Al	0.092	0.070	0.084	0.000	0.127	0.110	0.136	0.085	0.109	0.007	0.080	0.080	0.104
Fe ³⁺	0.006	0.008	0.012	0.007	0.003	0.002	0.007	0.004	0.016	0.005	0.012	0.012	0.016
Fe ²⁺	0.000	0.000	0.000	0.000	0.000	0.000	0.000	0.000	0.000	0.003	0.000	0.000	0.000
Mg	1.020	1.041	1.064	1.962	1.027	1.781	1.008	1.075	1.080	1.957	1.189	1.189	1.100
Ca	0.789	0.806	0.736	0.026	0.761	0.092	0.764	0.754	0.665	0.019	0.635	0.635	0.656
Na	0.081	0.052	0.079	0.007	0.070	0.011	0.079	0.069	0.079	0.004	0.064	0.064	0.070
K	0.019	0.027	0.047	0.007	0.023	0.007	0.009	0.021	0.061	0.006	0.025	0.025	0.064
Ba	0.000	0.000	0.000	0.000	0.000	0.000	0.000	0.000	0.000	0.000	0.000	0.000	0.000
Total	4.008	4.003	4.025	4.010	4.012	4.003	4.004	4.009	4.010	4.000	4.005	4.005	4.011
F	0.007	0.001	0.001	0.000	0.019	-	0.010	0.005	0.001	0.001	0.004	0.004	0.004

¹ Opx considered to be a quench product.

Table A6. Microprobe analyses of olivine, clinohumite, and chondrodite in experiments.

Exper.	TT352	TT350	TT353	BB173	BB438	GG765	BB361	GG524	GG748	TT270	BB692	GG733
T (°C)	1100	1100	1100	1200	1200	1200	1300	1300	1400	1400	1300	1400
P (GPa)	6.2	8.6	10.7	6.8	8.1	9.8	6.8	8.9	5.2	6.7	9.8	7.4
# Anal.	1	2	1	5	5	5	5	6	4	5	6	1
Phase	Chn	Chn	Chu	Chn	Chn	Chu	Chu	Ol	Ol	Ol	Ol	Ol
SiO ₂	33.01	36.15	35.51	33.95	35.17	38.63	38.97	42.15	42.92	42.42	42.73	42.32
TiO ₂	0.21	0.13	0.18	0.19	0.29	0.11	0.13	0.01	0.00	0.01	0.00	0.03
Al ₂ O ₃	0.38	0.43	1.63	0.07	0.18	0.22	0.08	0.04	0.09	0.06	0.06	0.07
FeO	0.62	0.39	1.48	0.88	0.31	0.48	0.36	0.51	0.03	0.73	0.56	0.51
MgO	54.39	59.65	52.93	59.96	59.18	56.31	59.68	56.37	57.31	56.84	55.64	57.12
CaO	0.10	0.11	0.25	0.08	0.09	0.10	0.10	0.05	0.12	0.06	0.06	0.08
BaO	0.03	0.03	0.01	0.01	0.01	0.01	0.01	0.00	0.01	0.01	0.00	0.01
Na ₂ O	0.03	0.03	0.05	0.02	0.02	0.03	0.02	0.01	0.01	0.01	0.00	0.02
K ₂ O	0.10	0.16	0.44	0.02	0.31	0.19	0.03	0.02	0.12	0.01	0.02	0.00
F	7.97	5.45	4.92	10.92	8.40	3.05	5.79	0.36	0.01	0.26	0.02	0.07
O=F	-3.36	-2.30	-2.07	-4.60	-3.54	-1.28	-2.44	-0.15	0.00	-0.11	-0.01	-0.03
H ₂ O*	1.17	2.84	0.41	0.16	1.33	1.42	0.23	-	-	-	-	-
Total	94.66	103.06	95.73	101.66	101.76	99.26	102.96	99.37	100.61	100.30	99.09	100.20
Si	2.000	2.002	3.892	1.910	1.976	4.059	3.939	0.998	1.000	0.996	1.011	0.993
Ti	0.010	0.005	0.015	0.008	0.012	0.009	0.010	0.000	0.000	0.000	0.000	0.000
Al	0.027	0.028	0.211	0.005	0.012	0.027	0.009	0.001	0.002	0.002	0.002	0.002
Fe	0.032	0.018	0.136	0.042	0.015	0.042	0.031	0.010	0.001	0.014	0.011	0.010
Mg	4.912	4.926	8.646	5.028	4.956	8.822	8.992	1.990	1.991	1.989	1.962	1.998
Ca	0.007	0.006	0.030	0.005	0.005	0.012	0.011	0.001	0.003	0.002	0.002	0.002
Ba	0.001	0.001	0.001	0.000	0.000	0.001	0.000	0.000	0.000	0.000	0.000	0.000
Na	0.004	0.003	0.010	0.002	0.002	0.005	0.004	0.001	0.001	0.000	0.000	0.001
K	0.008	0.011	0.061	0.001	0.022	0.025	0.004	0.001	0.004	0.000	0.001	0.000
Total	7	7	13	7	7	13	13	3.002	3.001	3.004	2.988	3.006
F	1.527	0.956	1.704	1.942	1.492	1.014	1.850	0.027	0.000	0.020	0.001	0.005
OH*	0.47	1.04	0.3	0.06	0.51	0.99	0.15	-	-	-	-	-
Cations	7	7	13	7	7	13	13	-	-	-	-	-
Oxygens	-	-	-	-	-	-	-	4	4	4	4	4
MF†/Si	2.47	2.47	2.26	2.65	2.52	2.29	2.29	2.00	1.99	2.01	1.95	2.02

* OH calculated to give 2 univalent anions and H₂O estimated from that.

† MF = Mg+Fe